

## Crustal evolution of Paleozoic-Mesozoic granitoid in Dakrong-A Luoi area, Truong Son belt, central Vietnam: evidence from zircon U-Pb geochronology, geochemistry, and Hf isotope composition


Nguyen Thi Dung, Tran Tuan Anh, Pham Trung Hieu, Pham Minh, Le Xuan Truong, Nguyen Trung Minh & Doan Dinh Hung

To cite this article: Nguyen Thi Dung, Tran Tuan Anh, Pham Trung Hieu, Pham Minh, Le Xuan Truong, Nguyen Trung Minh & Doan Dinh Hung (14 Feb 2024): Crustal evolution of Paleozoic-Mesozoic granitoid in Dakrong-A Luoi area, Truong Son belt, central Vietnam: evidence from zircon U-Pb geochronology, geochemistry, and Hf isotope composition, International Geology Review, DOI: [10.1080/00206814.2024.2315554](https://doi.org/10.1080/00206814.2024.2315554)

To link to this article: <https://doi.org/10.1080/00206814.2024.2315554>

 View supplementary material [↗](#)

---

 Published online: 14 Feb 2024.

---

 Submit your article to this journal [↗](#)

---

 View related articles [↗](#)

---

 View Crossmark data [↗](#)

---



# Crustal evolution of Paleozoic-Mesozoic granitoid in Dakrong-A Luoi area, Truong Son belt, central Vietnam: evidence from zircon U-Pb geochronology, geochemistry, and Hf isotope composition

Nguyen Thi Dung<sup>a,b</sup>, Tran Tuan Anh<sup>c</sup>, Pham Trung Hieu<sup>d,e</sup>, Pham Minh<sup>d,e</sup>, Le Xuan Truong<sup>f</sup>, Nguyen Trung Minh<sup>a</sup> and Doan Dinh Hung<sup>a</sup>

<sup>a</sup>Centre for Earth Sciences, Vietnam National Museum of Nature, Ha Noi, Vietnam; <sup>b</sup>Graduate University of Science and Technology, Vietnam; <sup>c</sup>Institute of Geological Sciences, Vietnam Academy of Science and Technology, Hanoi, Vietnam; <sup>d</sup>Faculty of Geology, VNU-HCM University of Science, Ho Chi Minh, Vietnam; <sup>e</sup>Vietnam National University Ho Chi Minh city, Ho Chi Minh City, Vietnam; <sup>f</sup>Faculty of Geosciences and Geoengineering/Center for Excellence in Analysis and Experiment, Hanoi University of Mining and Geology, Hanoi, Vietnam

## ABSTRACT

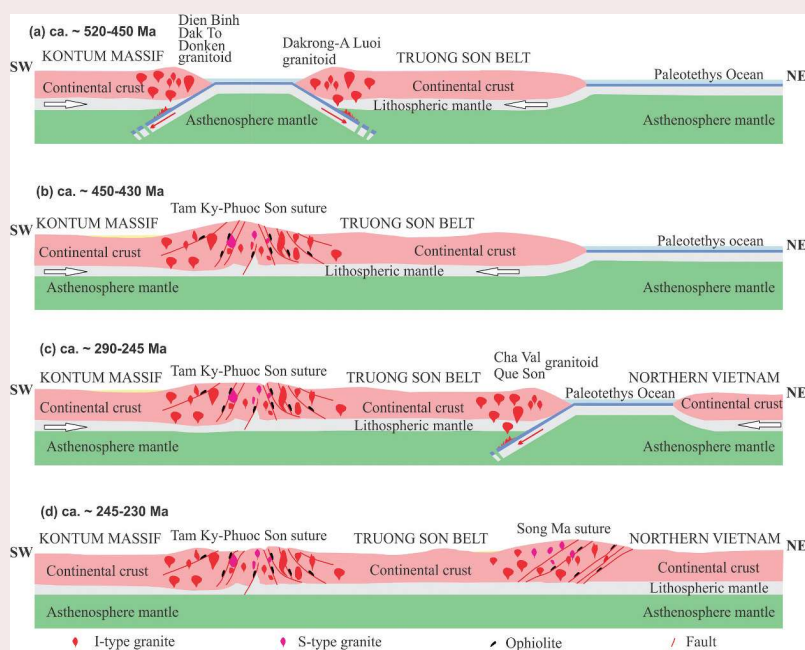
The Dakrong-A Luoi area is located in the South Truong Son belt in the Indochina block and has been affected by multiple stages of magmatic-metamorphic events. In this paper, Paleozoic-Mesozoic granitoids from the Dakrong-A Luoi area were studied using LA ICP-MS U-Pb zircon geochronologies, Hf isotopes on zircon and whole-rock geochemistry of the Paleozoic to examine the tectonic-magmatic history of the Southern Truong Son belt. The magmatism history of the area can be divided into three phases, at ~ 452 Ma (Ordovician), ~259 Ma (Permian), and ~ 243 Ma (Triassic). The Ordovician granites were exposed in the narrow belt of NW-SE trending, while the later two granite phases were exposed in E-W trending. The Ordovician granites show consistent LA-ICP-MS zircon  $\epsilon_{\text{Hf}}(t)$  values from + 6.2 to + 8.3. Their corresponding Hf model ages ( $T_{\text{DM}2}$ ) from 0.9 Ga to 1.0 Ga suggest that the Ordovician granite was derived from the partial melting of ancient crustal rocks, which is related to the subduction of the Tam Ky-Phuoc Son (TKPS) ocean beneath the Truong Son belt. The Permian granites have Hf isotopic natures ( $\epsilon_{\text{Hf}}(t)=-1.6$  to 1.3,  $T_{\text{DM}2} = 1.2-1.3$  Ga) of partial melting from ancient mantle components with minor Paleoproterozoic ancient continental crust. The Triassic granites have negative  $\epsilon_{\text{Hf}}(t)$  values ranging from -11.9 to -7.0 and Hf model ages of 1.7-2.0 Ga suggesting that they were a product of partial melting from the Paleoproterozoic crust, corresponding to subduction/collision of the Paleo-Tethys ocean beneath the Indochina block along the Song Ma suture.

## ARTICLE HISTORY

Received 25 August 2023  
Accepted 3 February 2024

## KEYWORDS

Geochemistry; Zircon U-Pb geochronology; Hf isotopic composition; Truong Son belt; Ordovician-Silurian; Permian-Triassic



**CONTACT** Pham Trung Hieu ✉ [pthieu@hcmus.edu.vn](mailto:pthieu@hcmus.edu.vn) Faculty of Geology, VNU-HCM University of Science, Ho Chi Minh, Vietnam

Supplemental data for this article can be accessed online at <https://doi.org/10.1080/00206814.2024.2315554>

© 2024 Informa UK Limited, trading as Taylor & Francis Group

## 1. Introduction

Southeast Asia consists of the Sibumasu, Indochina, and South China blocks that were marked by Changning-Menglian-Inthanon-Bentong and Ailaoshan-Song Ma suture zones (e.g. Metcalfe *et al.* 1998; Metcalfe 2006, 2013; Wang *et al.* 2020). The Indochina block is the largest structural unit in the Southeast Asia, encompassing parts of northeastern Thailand, Cambodia, the eastern peninsula of Malaysia, Laos, and Vietnam (Figure 1(a); Tri and Khuc 2011; Wang *et al.* 2020). It is located between Sibumasu to the Southwest and Yangtze, South China to the Northeast (Figure 1(a,b)); e.g. (Metcalfe 2006, 2013), bordering the East Sea of Vietnam (also called South China Sea) to the East. The Dakrong-A Luoi area is the farthest southern region of the Truong Son belt and adjacent to the Kontum massif in the eastern part of the Indochina block (Figure 1(a,b)).

The magmatic rocks in the Dakrong-A Luoi area recorded in geological maps scaled 1:200.000 (Huong Hoa-Hue-Da Nang map sheet) and 1:50.000 (Hue, Nam Dong, and Huong Hoa map sheets) (DGMVN 1995) include mafic to felsic rocks. The number of researches that have been conducted on magma formations, comprising the plutonic complexes of Dai

Loc (423–426 Ma, Hieu *et al.* 2016, pp. 415–420 Ma; Jiang *et al.* 2020, Ben Giang-Que Son 294 Ma; Sang 2011, and Hai Van 224–242 Ma; Hieu *et al.* 2015) in the region. The majority of these studies are primarily aimed in determining the composition of the granitoid rocks (for example, DGMVN 1995; Hoa *et al.* 2008a). There are not many studies that have been conducted on the ages and origins of granitoid formations. These studies have utilized K-Ar biotite, hornblende, and feldspar, as well as whole-rock Rb-Sr techniques, to date magmatic rocks. Some examples of these studies include Thúc and Trung (1995); Hoa *et al.* (2008a). According to previous research documents (DGMVN 1995; Tri and Khuc 2011; Tran *et al.* 2014; Minh *et al.* 2020; Nakano *et al.* 2021; Jiang *et al.* 2023) in this study area, there have been no quantitative studies on intrusive magmatic formations. Moreover, the Dakrong-A Luoi area has been affected by multiple stages of magmatic-tectonic events, hence, the current interpretation of the ages of magmatic rocks makes it difficult to comprehend the evolution of the continental crust in Vietnam in general and the A Luoi-Dakrong region in particular.

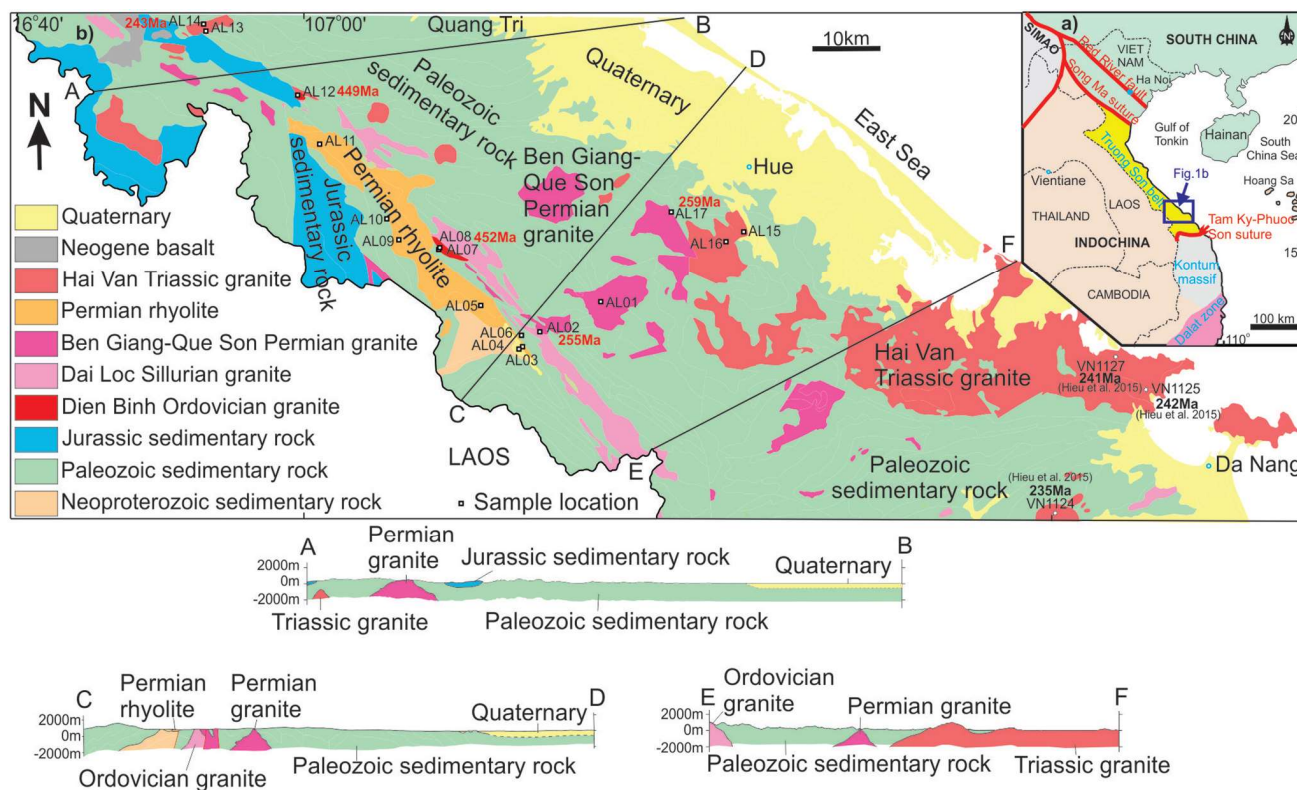


**Figure 1.** (a) Geological tectonic framework of Southeast Asia showing three major structural zones in the Indochina block (Minh *et al.* 2022). (b) Simplified geological map of the study area in the southern Truong Son belt and north Kontum Massif (modified after Trang 1994; DGMVN 1995). The geochronological data is compiled from this study and Hieu *et al.* (2015).

In this study, we present new findings on petrography, geochemistry, isotopic ages, and Hf isotopic composition in zircon and whole-rock for the granitoids from different magmatic-tectonic events in order to have a better understanding for the palaeogeographic reconstruction of the Dakrong-Aluoi area in the Truong Son belt with other terranes, including the Kontum massif and South China block.

## 2. Geological setting and petrography

The Indochina block in Vietnam was divided into three major structural zones: the Truong Son belt in the north, the Kontum massif in the centre, and the Dalat zone in the South. (Figure 1(a)). Dakrong-A Luoi area located in the South Truong Son belt, central Vietnam, has an extension of ~120 km from Quang Tri to Thua Thien Hue. The Truong Son belt is bounded by the Song Ma suture to the north and the TKPS suture to the South (Figure 1(a)). The basement rocks of the Truong Son belt include amphibole-biotite gneiss, quartz-biotite-garnet schist, and biotite-quartz schist, which occur in NW-SE trending (Tri and Khuc 2011). The plutonic-volcanic rocks in the Truong Son belt have widespread distribution and occurred in two main episodes: Ordovician-Silurian and Permian-Triassic (Hoa et al. 2008a, 2008b; Hieu et al. 2015, 2016, 2017; Wang et al. 2020). The common plutonic bodies are elongated and elliptical, with the NW-SE trend (Figure 1(b)). In this study, we mapped and collected 17 granitoid samples along national highways QL14 and QL49 and routes that cross-cut granitoid bodies in Dakrong-A Luoi area. The coordinates of sample locations are shown in Figure 1(b) and Table 1.

The Ordovician-Silurian granitoids in this study are classified as the Dai Loc complex with the composition of biotite granite and two-mica gneissoid granite (DGMVN 1995). However, our collected samples have lithological assemblages including granodiorite and biotite granite, exposed as small to medium bodies from the north to the south of the Truong Son belt, with an extension of ~200 km<sup>2</sup>. In the Dakrong-A Luoi area, they intruded into the Early Paleozoic Sequences and are locally overlain by Jurassic sediments (Figures 1(b) and 2(a,b)). The granitoids mainly consist of plagioclase (40–50%, commonly in plate form), quartz (25–30%, commonly in subhedral crystals), K-feldspar (10–16%), and biotite (5–10%) (Figure 3(a,b)) of which K-feldspar is strongly kaolinized. Plagioclase is found in shapes of euhedral and subhedral grains (0.5–1.5 mm) with polysynthetic twinning. Plagioclase is partially altered to sericite in some samples. Quartz is made up of anhedral grains (0.2–1.2 mm). The grains of quartz exhibit undulose extinction frequently due to their stretching,

folding, and widespread recrystallization. Biotite is found in the form of euhedral sheet crystals (0.3–1.5 mm) with minor fading or chlorite alteration. The accessory minerals recorded in these rocks are apatite and zircon. With the lithological assemblages and age of formation in this study, the Ordovician-Silurian granitoid rocks are similar to the Dien Binh complex (Trong et al. 2021).

The Permian-Triassic granitoids include the Ben Giang-Que Son and Hai Van complexes. They have been recorded in an area of 500 km<sup>2</sup> and occurred as NW-SE trend. These rocks mainly include granodiorite and granite with massive textures (Figure 2(c–f)), in which the granite is divided into I- and S-type series (Figure 3). The mineralogical composition from Ben Giang-Que Son complex includes plagioclase (40–45%), hornblende (20–35%), quartz (0–15%), biotite (10–20%), and K-feldspar (0–5%) (Figure 3(c–e)). The presence of hydrous phases like as biotite and hornblende suggests that the granitoids formed in a water-rich original magma, corresponding to I-type granite. Plagioclase grains (0.4–2 mm) are generally euhedral in form, with polysynthetic twins. Hornblende grains (0.5–2 mm) range from euhedral to subhedral in shape and frequently contain quartz and biotite inclusions. Euhedral to subhedral quartz grains have a size of 0.3–1.8 mm. K-feldspar is anhedral in shape (0.2–1 mm) and partially kaolinized. The mineralogical composition from Hai Van complex (i.e. two-mica) granite includes plagioclase (40–45%), quartz (10–20%), potassium feldspar (10–25%), biotite (5–15%), and muscovite (2–3%), corresponding to the S-type granite (Figure 3(f)). Plagioclase grains (0.75–3 mm) are the most abundant mineral, are usually euhedral in shape and have polysynthetic twins. Potassium feldspar grain (0.2–2 mm) is anhedral in shape and always kaolinized. Quartz is commonly euhedral to subhedral with a length of 0.5–1 mm. Some biotite grains (0.5–2 mm) have been partially altered to chlorite.

## 3. Analytical methods

*Whole rock geochemistry:* Eight Permian-Triassic samples (AL01, AL02, AL13, AL14, AL17, AL01(R), AL15, and AL16) and three Ordovician-Silurian samples (AL08, AL08.1 and AL12) of the Dakrong-A Luoi area, Truong Son belt were collected for this study. All analyses were conducted at the China Geoscience University, Wuhan, China. The samples were crushed and then powdered to the grain size < 200 μm. Major elemental contents were obtained by X-ray fluorescence spectrometry (XRF). Standard samples GBW07103, GBW07105 and GBW07111 were used to manage the analytical precision. An Agilent 7500a

**Table 1.** Ages of Ordovician-Silurian and Permian-Triassic volcanic and plutonic in Indochina block. Locations are shown in Figure 13(b).

Sample no.	Rock type	Age (Ma)	Method	Material	Reference
AL08	Granite	454 ± 6.5	LA-ICP-MS	zircon	This study
AL12	Granite	455 ± 6.6	LA-ICP-MS	zircon	This study
AL02	Granite	257 ± 3.7	LA-ICP-MS	zircon	This study
AL17	Granite	261 ± 3.7	LA-ICP-MS	zircon	This study
AL14	Granite	246 ± 3.0	LA-ICP-MS	zircon	This study
<b>Ordovician-Silurian event</b>					
KT29	Diorite	473 ± 3	LA-ICP-MS	zircon	Trong <i>et al.</i> (2021)
KT31	Diorite	485 ± 2	LA-ICP-MS	zircon	Trong <i>et al.</i> (2021)
KT47	Diorite	457 ± 6	LA-ICP-MS	zircon	Trong <i>et al.</i> (2021)
KT51	Granite	453 ± 6	LA-ICP-MS	zircon	Trong <i>et al.</i> (2021)
KT33	Granite	422 ± 6	LA-ICP-MS	zircon	Trong <i>et al.</i> (2021)
KT36	Granite	422 ± 5	LA-ICP-MS	zircon	Trong <i>et al.</i> (2021)
V1722	Granitic gneiss	445 ± 7.3	LA-ICP-MS	zircon	Minh <i>et al.</i> (2020)
V1723	Granitic gneiss	453 ± 16	LA-ICP-MS	zircon	Minh <i>et al.</i> (2020)
V1724	Granitic gneiss	454.4 ± 6.1	LA-ICP-MS	zircon	Minh <i>et al.</i> (2020)
V1726	Granitic gneiss	454 ± 14	LA-ICP-MS	zircon	Minh <i>et al.</i> (2020)
17KT12-1	Granite	445 ± 3	LA-ICP-MS	zircon	Jiang <i>et al.</i> (2020)
17KT12-2	Granite	445.8 ± 4.4	LA-ICP-MS	zircon	Jiang <i>et al.</i> (2020)
16KT24-2	Granite	451.8 ± 4.3	LA-ICP-MS	zircon	Jiang <i>et al.</i> (2020)
16KT24-7	Granite	445 ± 3.6	LA-ICP-MS	zircon	Jiang <i>et al.</i> (2020)
16KT22-1	Granite	419.8 ± 2.5	LA-ICP-MS	zircon	Jiang <i>et al.</i> (2020)
16KT23-1	Granite	414.8 ± 3.1	LA-ICP-MS	zircon	Jiang <i>et al.</i> (2020)
CG001	Diorite	470.0 ± 1.9	LA-ICP-MS	zircon	Gardner <i>et al.</i> (2017)
CG062	Rhyolitic tuff	476.1 ± 1.5	LA-ICP-MS	zircon	Gardner <i>et al.</i> (2017)
DLT02	Granite	426.9 ± 9.9	LA-ICP-MS	zircon	Hieu <i>et al.</i> (2016)
DLT07	Granite	423 ± 2	LA-ICP-MS	zircon	Hieu <i>et al.</i> (2016)
V1104	Quartz diorite	479 ± 3	LA-ICP-MS	zircon	Hieu <i>et al.</i> (2015)
VN13	Gneiss	407 ± 11	SHRIMP	zircon	Carter <i>et al.</i> (2001)
VN610	Gneiss	418 ± 8	SHRIMP	zircon	Carter <i>et al.</i> (2001)
VN386	Granodiorite	451 ± 3	LA-ICP-MS	zircon	Nagy <i>et al.</i> (2001)
<b>Permian-Triassic event</b>					
DK26	Granite	258.4 ± 1.6	LA-ICP-MS	zircon	Hoang <i>et al.</i> (2023)
DK03	Granite	245.2 ± 2.2	LA-ICP-MS	zircon	Hoang <i>et al.</i> (2023)
DK34	Granite	243.6 ± 2.5	LA-ICP-MS	zircon	Hoang <i>et al.</i> (2023)
DH07	Granite	240.3 ± 2.6	LA-ICP-MS	zircon	Hung <i>et al.</i> (2022)
DH08	Granite	250.8 ± 4.2	LA-ICP-MS	zircon	Hung <i>et al.</i> (2022)
DH08-1	Granite	240.1 ± 2.7	LA-ICP-MS	zircon	Hung <i>et al.</i> (2022)
DH14	Granite	229.4 ± 4.0	LA-ICP-MS	zircon	Hung <i>et al.</i> (2022)
DH16	Granite	237.5 ± 2.3	LA-ICP-MS	zircon	Hung <i>et al.</i> (2022)
DH20	Granite	244.0 ± 3.0	LA-ICP-MS	zircon	Hung <i>et al.</i> (2022)
DH26	Granite	233.1 ± 5.2	LA-ICP-MS	zircon	Hung <i>et al.</i> (2022)
DH47-1	Granite	240.2 ± 2.0	LA-ICP-MS	zircon	Hung <i>et al.</i> (2022)
KTM-GbDi1918	Diorite	248.9 ± 1.9	LA-ICP-MS	zircon	Minh <i>et al.</i> (2022)
KTMGbDi1921	Quartz diorite	258.0 ± 2.9	LA-ICP-MS	zircon	Minh <i>et al.</i> (2022)
KTM-Di1922	Diorite	254.0 ± 1.7	LA-ICP-MS	zircon	Minh <i>et al.</i> (2022)
V1703	Granitoid	236.9 ± 4.5	LA-ICP-MS	zircon	Hieu <i>et al.</i> (2020)
V1705	Granitoid	241.7 ± 4.7	LA-ICP-MS	zircon	Hieu <i>et al.</i> (2020)
V1706	Granitoid	237.4 ± 8.3	LA-ICP-MS	zircon	Hieu <i>et al.</i> (2020)
V1708	Granitoid	235.8 ± 5.1	LA-ICP-MS	zircon	Hieu <i>et al.</i> (2020)
MLT08	Monzogranite	251 ± 3	LA-ICP-MS	zircon	Thanh <i>et al.</i> (2019)
MLT09	Granodiorite	247.4 ± 2.8	LA-ICP-MS	zircon	Thanh <i>et al.</i> (2019)
MLT34	Monzogranite	242 ± 2.6	LA-ICP-MS	zircon	Thanh <i>et al.</i> (2019)
MLT42	Monzogranite	235 ± 3.1	LA-ICP-MS	zircon	Thanh <i>et al.</i> (2019)
15NL-14B	Granodiorite	281 ± 1	LA-ICP-MS	zircon	Qian <i>et al.</i> (2019)
15NL-28C	Hornblende granite	276 ± 1	LA-ICP-MS	zircon	Qian <i>et al.</i> (2019)
15NL-45A	Granodiorite	221 ± 1	LA-ICP-MS	zircon	Qian <i>et al.</i> (2019)
15NL-27A	Hornblende granite	234 ± 1	LA-ICP-MS	zircon	Qian <i>et al.</i> (2019)
15NL-23A	Biotite granite	274 ± 1	LA-ICP-MS	zircon	Qian <i>et al.</i> (2019)
15NL-31A	Biotite granite	273 ± 1	LA-ICP-MS	zircon	Qian <i>et al.</i> (2019)
15NL-68A	Biotite granite	272 ± 1	LA-ICP-MS	zircon	Qian <i>et al.</i> (2019)
15NL-69A	Biotite granite	271 ± 1	LA-ICP-MS	zircon	Qian <i>et al.</i> (2019)
15NL-43A	Biotite granite	260 ± 1	LA-ICP-MS	zircon	Qian <i>et al.</i> (2019)
15NL-60A	Biotite granite	258 ± 1	LA-ICP-MS	zircon	Qian <i>et al.</i> (2019)
15NL-61A	Biotite granite	260 ± 1	LA-ICP-MS	zircon	Qian <i>et al.</i> (2019)
15NL-64A	Rhyolite	261 ± 1	LA-ICP-MS	zircon	Qian <i>et al.</i> (2019)
V0738	Quartz diorite	262 ± 4	LA-ICP-MS	zircon	Hieu <i>et al.</i> (2017)
V0741	Granite	260 ± 5	LA-ICP-MS	zircon	Hieu <i>et al.</i> (2017)
V0821	Tonalite	256 ± 7	LA-ICP-MS	zircon	Hieu <i>et al.</i> (2017)
V0856	Granite	263 ± 5	LA-ICP-MS	zircon	Hieu <i>et al.</i> (2017)
V0903	Granodiorite	233 ± 4	LA-ICP-MS	zircon	Hieu <i>et al.</i> (2017)

(Continued)

**Table 1.** (Continued).

Sample no.	Rock type	Age (Ma)	Method	Material	Reference
V0905	Granodiorite	231 ± 4	LA-ICP-MS	zircon	Hieu <i>et al.</i> (2017)
V0908	Biotite granite	244 ± 5	LA-ICP-MS	zircon	Hieu <i>et al.</i> (2017)
V1106	Granite	239 ± 6	LA-ICP-MS	zircon	Hieu <i>et al.</i> (2017)
R11	Rhyolite	256 ± 7	LA-ICP-MS	zircon	Hieu <i>et al.</i> (2017)
LH16	Tonalite	234 ± 3.5	LA-ICP-MS	zircon	Wang <i>et al.</i> (2016)
LC16	Monzogranite	234.3 ± 1.5	LA-ICP-MS	zircon	Wang <i>et al.</i> (2016)
LH13	Tonalite	236.3 ± 3.2	LA-ICP-MS	zircon	Wang <i>et al.</i> (2016)
LH11	Tonalite	238.6 ± 3.2	LA-ICP-MS	zircon	Wang <i>et al.</i> (2016)
LT4	Granodiorite	240.1 ± 1.6	LA-ICP-MS	zircon	Wang <i>et al.</i> (2016)
LH4	Granodiorite	244.5 ± 2	LA-ICP-MS	zircon	Wang <i>et al.</i> (2016)
LT6	Granodiorite	244.8 ± 3.9	LA-ICP-MS	zircon	Wang <i>et al.</i> (2016)
LC1	Monzogranite	245.1 ± 2.9	LA-ICP-MS	zircon	Wang <i>et al.</i> (2016)
LC8	Monzogranite	245.9 ± 2.8	LA-ICP-MS	zircon	Wang <i>et al.</i> (2016)
LH1	Granodiorite	249 ± 1.9	LA-ICP-MS	zircon	Wang <i>et al.</i> (2016)
LH5	Granodiorite	249.9 ± 1.8	LA-ICP-MS	zircon	Wang <i>et al.</i> (2016)
LC17	Monzogranite	251.2 ± 2.1	LA-ICP-MS	zircon	Wang <i>et al.</i> (2016)
LC12	Monzogranite	253.3 ± 1.8	LA-ICP-MS	zircon	Wang <i>et al.</i> (2016)
LT1	Granodiorite	254.4 ± 2.5	LA-ICP-MS	zircon	Wang <i>et al.</i> (2016)
LC6	Monzogranite	254.9 ± 1.6	LA-ICP-MS	zircon	Wang <i>et al.</i> (2016)
LT3	Granodiorite	256.4 ± 3.1	LA-ICP-MS	zircon	Wang <i>et al.</i> (2016)
V1102-3	Granite	224 ± 4.6	LA-ICP-MS	zircon	Hieu <i>et al.</i> (2015)
V1102	Granite	234.7 ± 3.7	LA-ICP-MS	zircon	Hieu <i>et al.</i> (2015)
V1124	Granite	235 ± 14	LA-ICP-MS	zircon	Hieu <i>et al.</i> (2015)
V1127	Granite	241.4 ± 2	LA-ICP-MS	zircon	Hieu <i>et al.</i> (2015)
V1125	Granite	242.1 ± 4.8	LA-ICP-MS	zircon	Hieu <i>et al.</i> (2015)
V1114	Granite	242 ± 2.4	LA-ICP-MS	zircon	Hieu <i>et al.</i> (2015)
VN12-066	Granodiorites	242.2 ± 1.3	LA-ICP-MS	zircon	Shi <i>et al.</i> (2015)
VN12-050	Plagiogranite	251.8 ± 1.9	LA-ICP-MS	zircon	Shi <i>et al.</i> (2015)
VN12-025	Rhyolite	251.9 ± 1.7	LA-ICP-MS	zircon	Shi <i>et al.</i> (2015)
VN12-022	Monzogranite	253.4 ± 1.5	LA-ICP-MS	zircon	Shi <i>et al.</i> (2015)
VN12-056	Monzogranites	260.9 ± 1.6	LA-ICP-MS	zircon	Shi <i>et al.</i> (2015)
JH0804	Granitic gneiss	244.5 ± 2.5	LA-ICP-MS	zircon	Tran <i>et al.</i> (2014)
JH0822	Granite	245.9 ± 1.5	LA-ICP-MS	zircon	Tran <i>et al.</i> (2014)
HRDD221	Paragneiss	247.7 ± 1.9	LA-ICP-MS	zircon	Tran <i>et al.</i> (2014)
JH0810	Granodiorite	252.1 ± 1.5	LA-ICP-MS	zircon	Tran <i>et al.</i> (2014)
KD10-32/1	Diorite	255.6 ± 3.4	LA-ICP-MS	zircon	Tran <i>et al.</i> (2014)
DCL09	Dioritic gneiss	257.2 ± 4.4	LA-ICP-MS	zircon	Tran <i>et al.</i> (2014)
VT 225	Granite	225 ± 3	LA-ICP-MS	zircon	Roger <i>et al.</i> (2014)
VT 226	Granite	230 ± 1	LA-ICP-MS	zircon	Roger <i>et al.</i> (2014)
11SM5I	Eclogite	230.5 ± 8.2	SHRIMP	zircon	Zhang <i>et al.</i> (2013)
V0829	Quartz diorite	270.9 ± 3.3	LA-ICP-MS	zircon	Liu <i>et al.</i> (2012)
	Granite	260 ± 4	SHRIMP	zircon	Hoa <i>et al.</i> 2008a
VN 09	Gneiss	244 ± 7	SHRIMP	zircon	Carter <i>et al.</i> (2001)

inductively coupled with a plasma mass spectrometry was used to analyse trace element values. In this step, the standard samples BHVO-2, AGV-2 and OU-6 were used to manage the analytical precisions. Based on the analyses of standard samples, errors were less than 5% in precision for major and trace element contents. The details of the analytical method were described in Hieu *et al.* (2020).

**Geochronology:** The LA ICP-MS U-Pb zircon ages for five samples (AL08, AL12, AL02, AL14, and AL17) from the Dakrong-A Luoi region, Truong Son belt were conducted at the AAC (Advanced Analytical Centre), James Cook University, Townsville. Zircon grains were separated from rock powders after magnetic and heavy liquid separation. Representative zircon grains for each sample were handpicked using a microscope before being mounted in a 2.5 cm epoxy resin puck. To detect internal textures and classify zircon types, the zircon grains were analysed with cathodoluminescence (CL)

imaging using the Jeol JSM5410LV scanning electron microscope. The individual zircon grains were analysed for U-Pb isotopic composition based on a Geolas Pro 193 nm ArF excimer laser system connected with a Bruker 820-MS ICP-MS. The ablation was carried out using a laser with an energy density of 2 J/cm<sup>2</sup> on a spot size of 25 µm and at a rate of 5 Hz. The ICP-MS was tuned to ensure low oxide production levels (ThO/Th < 0.5%) and approximately equal sensitivity of U, Th, and Pb to minimize isotope fractionation (Pettke 2008). The obtained isotopic composition includes <sup>29</sup>Si, <sup>90</sup>Zr, <sup>202</sup>Hg, <sup>204</sup>Pb, <sup>206</sup>Pb, <sup>207</sup>Pb, <sup>208</sup>Pb, <sup>232</sup>Th, <sup>235</sup>U, and <sup>238</sup>U. The final statistical plotting was done using Isoplot/Ex (Ludwig 2003). The details for this analytical technique were presented in Le *et al.* (2021).

**Lu-Hf isotopes:** All Lu-Hf isotopic analyses for five samples (AL12, AL14, and AL17) from the Dakrong-A Luoi region, Truong Son belt were conducted in at the China Geoscience University, Wuhan, China using a Thermo

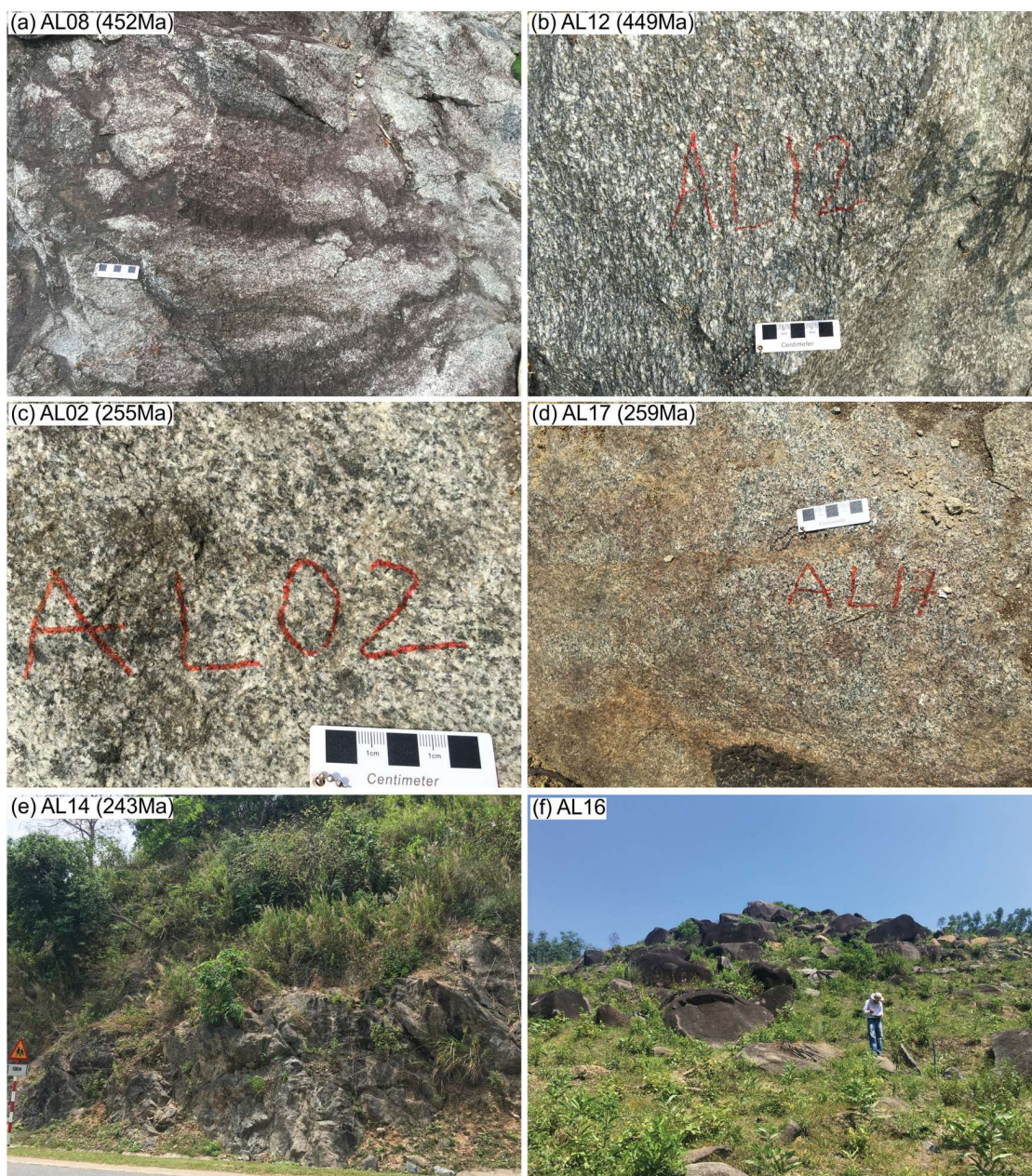


**Figure 2.** Fieldwork photographs of the Dakrong-A Luoi plutonic rocks in the South Truong Son belt. (a) biotite granite from Dien Binh complex, (b) granodiorite from Dien Binh complex, (c, d) granodiorite from Ben Giang-Que Son complex, (e, f) biotite granite from Hai Van complex.

Finnigan Neptune multi-collector ICP-MS and a Geolas CQ 193 nm laser ablation system. The beam had a diameter of 44  $\mu$ m and a pulse frequency of 10 Hz. As a benchmark for purity, the zircon Muk Tank was analysed. Wu *et al.* (2006) have disclosed analytical methods and an interference correction technique for  $^{176}\text{Yb}/^{176}\text{Hf}$  that are comparable to what we have used. Initial  $^{176}\text{Hf}/^{177}\text{Hf}$  ratios were computed using the  $^{176}\text{Lu}$  decay constant of  $1.8651011 \text{ year}^{-1}$  (Scherer *et al.* 2001). Using the reported chondritic values of  $^{176}\text{Lu}/^{177}\text{Hf} = 0.0336$  and  $^{176}\text{Hf}/^{177}\text{Hf} = 0.282785$  (Bouvier *et al.* 2008), we can compute the Hf values. Using a ratio

of  $^{176}\text{Lu}/^{177}\text{Hf} = 0.015$ , we were able to determine the age of the second stage of the Hf model ( $T_{DM2}$ ) based on the average continental crust (Griffin *et al.* 2002).

## 4. Study results

### 4.1. Geochemistry

Major and trace element compositions from Ordovician-Silurian and Permian-Triassic granitoid in the Dakrong-A Luoi area, Truong Son belt are presented in Supp. Tables s1 and s2, respectively.

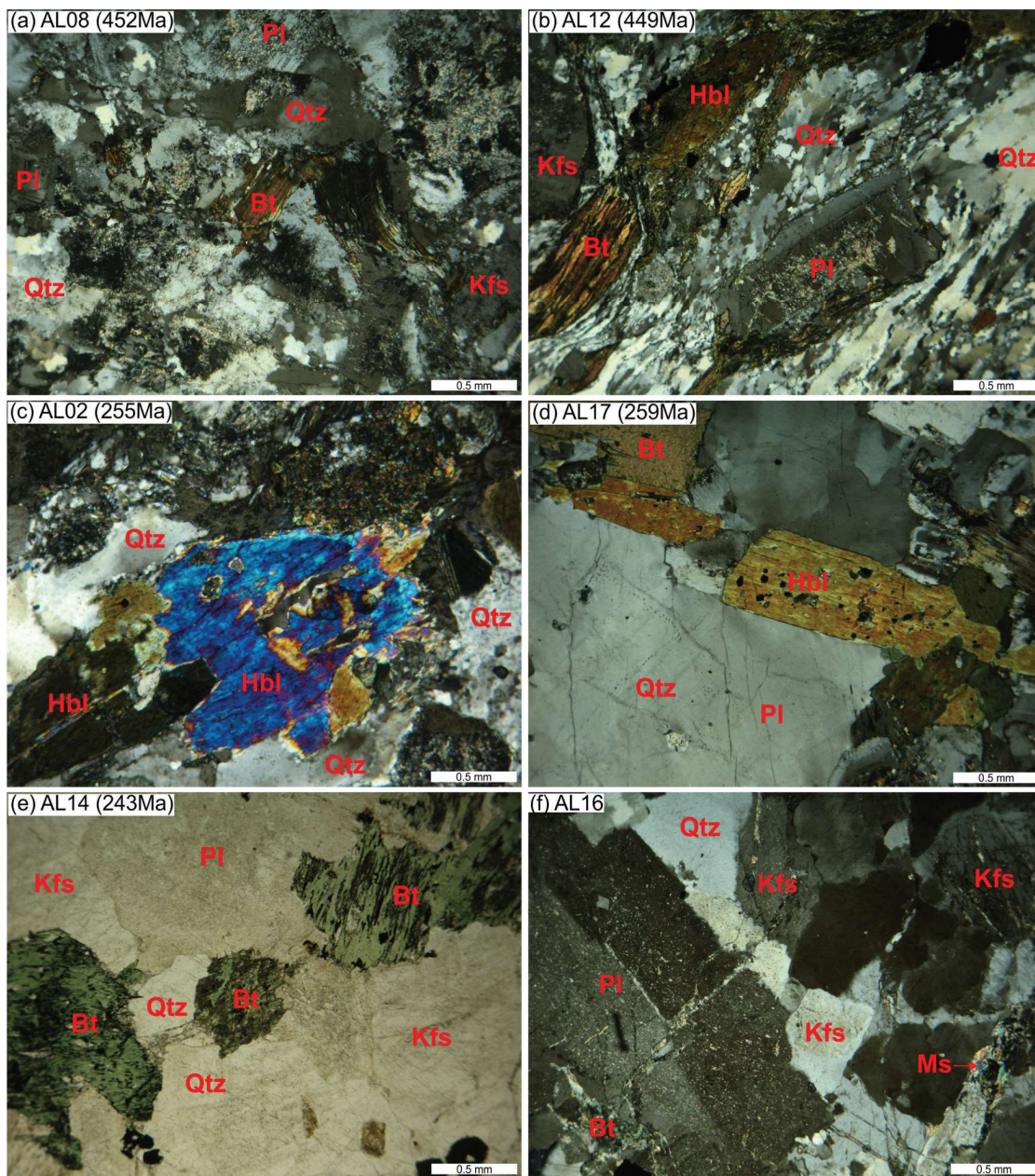


**Figure 3.** Thin-section photographs of the Dakrong-A Luoi plutonic rocks in the south Truong Son belt. (a) biotite granite from Dien Binh complex, (b) granodiorite from Dien Binh complex, (c, d) granodiorite from Ben Giang-Que Son complex, (e, f) biotite granite from Hai Van complex. Mineral abbreviations: Bt: biotite, Hbl: hornblende, K-feldspar: kfs, Muscovite: ms, pl: plagioclase, Qtz: quartz.

#### 4.1.1. Dien Binh Ordovician granitoids

The Dien Binh Ordovician granitoids in the study area are mainly composed of  $\text{SiO}_2$  (63.77–70.76 wt%),  $\text{Al}_2\text{O}_3$  (13.86–16.73 wt%),  $\text{TiO}_2$  (0.42–0.66 wt%), and  $\text{FeO}^t$  (4.37–4.71 wt%) (Supp Figure S1(a–i)). On Harker diagrams, the trend of the I- and S-type granite is different (Supp Figure S1(a–i)). The  $\text{TiO}_2$ ,  $\text{Al}_2\text{O}_3$ ,  $\text{MnO}$ ,  $\text{Na}_2\text{O}$  and  $\text{K}_2\text{O}$  compositions of the I- and S-type granites are nearly invariable while the  $\text{Fe}_2\text{O}_3^t$ ,  $\text{MgO}$ , and  $\text{CaO}$  contents of the I- and S-type granites decline with increasing

$\text{SiO}_2$ . Besides, the  $\text{P}_2\text{O}_5$  contents of I-type granites decline with increasing  $\text{SiO}_2$ , but the  $\text{P}_2\text{O}_5$  compositions of S-type granites increase with increasing  $\text{SiO}_2$ . Loss on ignition (LOI) values vary from 0.98 to 2.51 wt%. Most of the samples are geochemically plotted in domains of granodiorite and granite fields (Figure 4(a)). Normative mineral compositions by CIPW major element indicate that the mineralogy of Ordovician-Silurian granitoids includes plagioclase, K-feldspar, quartz, hornblende, and biotite that are similar to those observed in the



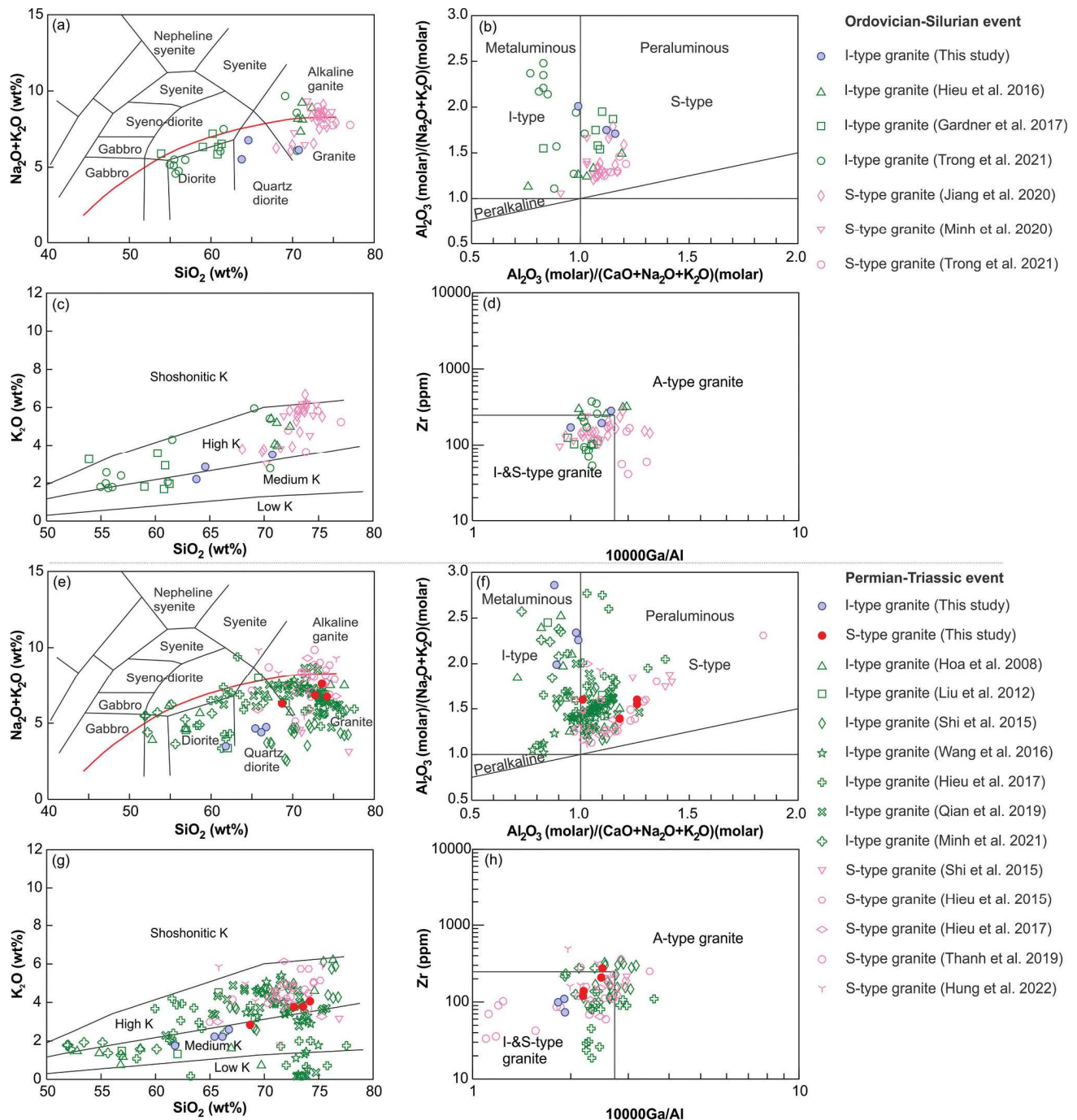


**Figure 4.** Rock classification for the dakrong-A luoi plutonic rocks in the South Truong Son belt: (a,e) QAPF diagram (Le Bas and Streckeisen 1991); (b,f) A/CNK vs A/NK diagram (Maniar and Piccoli 1989); (c,g)  $K_2O$  vs  $SiO_2$  diagram (Peccerillo and Taylor 1976); (d,h) Zr versus  $10,000 \times Ga/Al$  diagram (Whalen *et al.* 1987). Literature data is derived from Hoa *et al.* (2008a); Liu *et al.* (2012); Shi *et al.* (2015); Hieu *et al.* (2015) (Hieu *et al.* 2016); (Hieu *et al.* 2017); Wang *et al.* (2016); Gardner *et al.* (2017); Qian *et al.* (2019); Thanh *et al.* (2019); Minh *et al.* (2021); Minh *et al.* (2020); Jiang *et al.* (2020); Trong *et al.* (2021); Hung *et al.* (2022) and this study.

microscope (Supp. Table s1). On Harker diagrams, the variation in composition of the I-type granite shows different trends compared to that of the S-type granite (Supp Figure S1(a-i)). The  $Na_2O$  and  $MnO$  contents are nearly invariable, while the contents of  $TiO_2$ ,  $Al_2O_3$ ,  $Fe_2O_3$ ,  $MgO$ ,  $CaO$ , and  $P_2O_5$  are negatively correlated to

$SiO_2$  contents, except for the  $K_2O$  which is positively related to  $SiO_2$ . The A/CNK ratios range from 0.99 to 1.16, and are plotted in the peraluminous domain (Figure 4(b)). The  $K_2O$  contents (2.20 to 3.51 wt%) belong to the medium-high potassium domain (Figure 4(c)). According to the granite classification diagram, most of

the samples were plotted in I-type and S-type granite domains (Figure 4(d)) while the major elements of the granitoid from the study area (Figure 4) are comparable to those from the I-type granite in the Kontum area (Gardner *et al.* 2017; Jiang *et al.* 2020).

The total values of rare earth elements ( $\Sigma$ REE) from the Ordovician-Silurian granitoid vary from 147.04 to 246.28 ppm. Light rare earth element values ( $\Sigma$ LREE) range from 133.98 to 221.97 ppm, while heavy rare earth element values ( $\Sigma$ HREE) range from 11.29 to 24.31 ppm (Supp. Table 2). Chondrite-normalized REE patterns show strongly heterogeneous Eu anomalies ( $\text{Eu}/\text{Eu}^* = 0.59\text{--}0.92$ ; Figure 5(a)). Primitive mantle-normalized REE patterns exhibit the positive anomalies of Cs, U, K, Pb, and Nd and the negative anomalies of Ba, Nb, Ce, P, Zr, and Ti trace elements (Figure 5(b,c)). The negative anomaly of Eu and Ba could be caused by the fractionation of the plagioclase and K-feldspar crystallizations. The temperature of zircon crystallization in the Ordovician-Silurian granitoid, calculated using (Watson and Harrison 1983) zircon thermometer, varies from 785.56 to 848.09°C (Figure 6(a)). The Dien Binh Ordovician granitoid tends to indicate an I-type granite. However, the trend is not apparent. According to the tectonic classification diagrams from (Pearce *et al.* 1984), granitoid is commonly plotted in the subduction

zone (Figure 6(c,d)). The trace element contents of the Ordovician-Silurian granitoid in the study area (Figures 5 and 6) are comparable to those of 460–470 Ma I-type granite in the Kontum massif.

#### 4.1.2. Ben Giang-Que Son Permian granitoid and Hai Van Triassic two-mica granite

The composition of Permian-Triassic granitoids in the study area is characterized by  $\text{SiO}_2$  (61.80–74.20 wt%),  $\text{Al}_2\text{O}_3$  (12.66–14.65 wt%),  $\text{TiO}_2$  (0.23–0.60 wt%) and  $\text{FeO}^t$  (1.28–7.63 wt%) (Supp Figure S1(j-r)). On Harker diagrams, the trend of the I- and S-type granite is different (Supp Figure S1(j-r)). The  $\text{TiO}_2$ ,  $\text{Al}_2\text{O}_3$ , MnO, MgO and CaO contents of the I- and S-type granites decline with increasing  $\text{SiO}_2$  while the  $\text{K}_2\text{O}$  and  $\text{Na}_2\text{O}$  compositions of the I- and S-type granites are nearly invariable. Furthermore, the  $\text{Fe}_2\text{O}_3t$  and  $\text{P}_2\text{O}_5$  contents of I-type granites decline with increasing  $\text{SiO}_2$ , but the  $\text{P}_2\text{O}_5$  compositions of S-granites increase with increasing  $\text{SiO}_2$ . The LOI values vary from 0.64 to 3.33 wt%. Most of the samples were plotted in the granodiorite and granite domains (Figure 4(c)). CIPW mineral normalization of major elements suggests that the mineral composition of Permian-Triassic granitoids includes plagioclase,

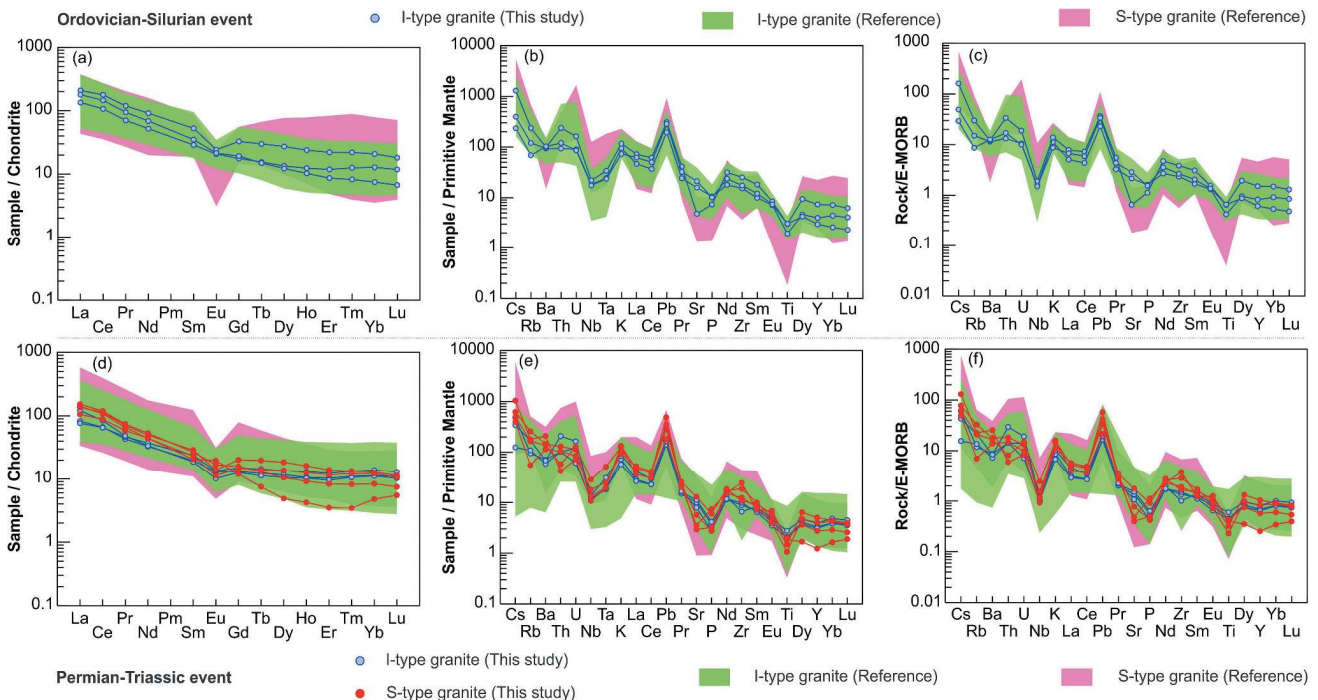


**Figure 5.** (a,d) Chondrite-normalized REE patterns, (b,e) primitive mantle-normalized multi-element patterns and (c,f) E-MORB-normalized multi-element patterns for the dakrong-A luoi plutonic rocks in the South Truong Son belt. Normalization values are from Sun and McDonough (1989). Literature data is derived from Hoa *et al.* (2008a); Liu *et al.* (2012); Shi *et al.* (2015); Hieu *et al.* (2015) (Hieu *et al.* 2016); (Hieu *et al.* 2017); Wang *et al.* (2016); Gardner *et al.* (2017); Qian *et al.* (2019); Thanh *et al.* (2019); Minh *et al.* (2021); Minh *et al.* (2020); Jiang *et al.* (2020); Trong *et al.* (2021); Hung *et al.* (2022) and this study.

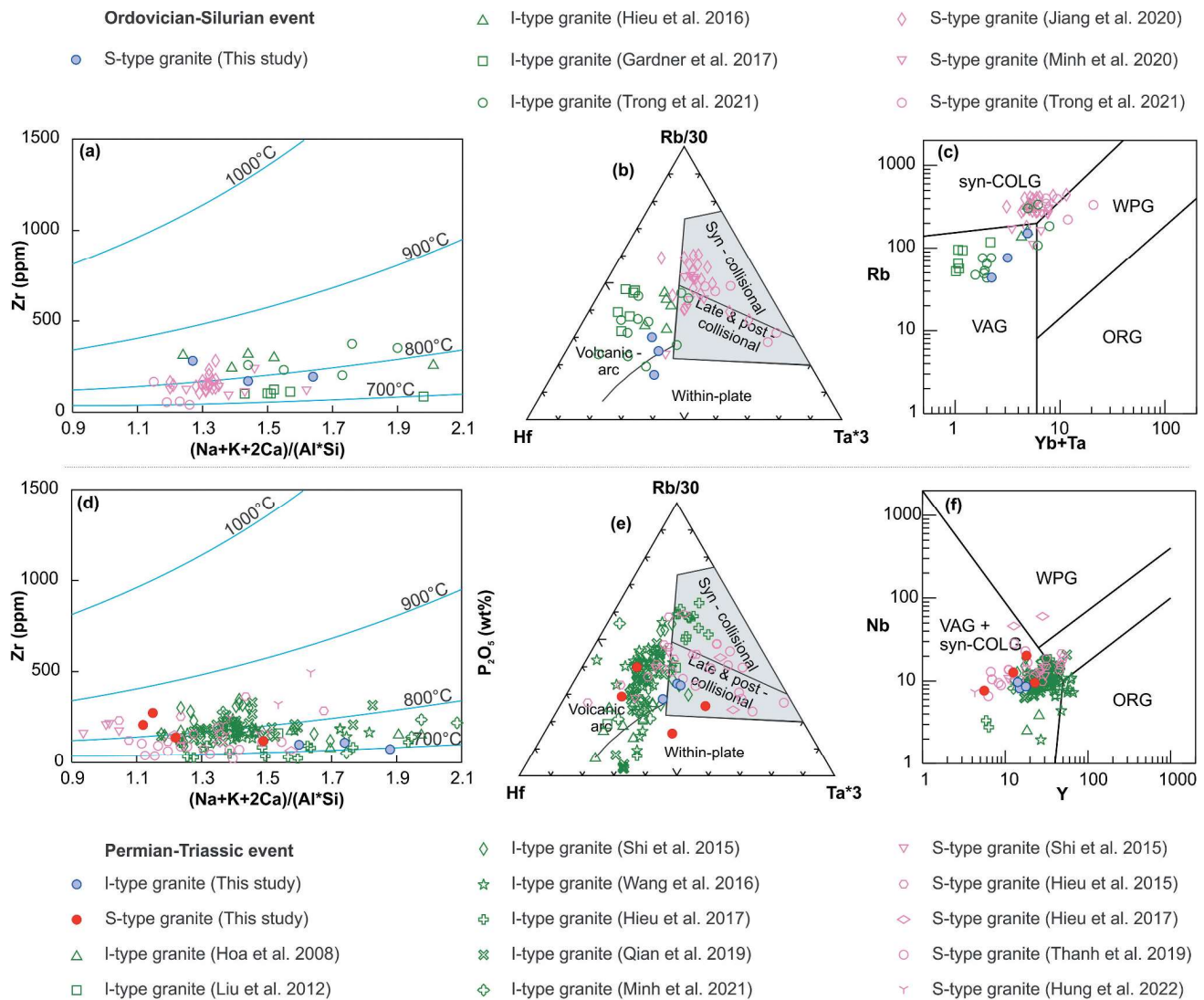


**Figure 6.** (a,d) zircon saturation thermometer (Watson and Harrison 1983) and (b,c,e,f) geotectonic classification diagrams based on trace element compositions (Pearce *et al.* 1984) for the Dakrong-A Luoi plutonic rocks in the South Truong Son belt. Literature data is derived from Hoa *et al.* (2008a); Liu *et al.* (2012); Shi *et al.* (2015); Hieu *et al.* (2015) (Hieu *et al.* 2016); (Hieu *et al.* 2017); Wang *et al.* (2016); Gardner *et al.* (2017); Qian *et al.* (2019); Thanh *et al.* (2019); Minh *et al.* (2021); Minh *et al.* (2020); Jiang *et al.* (2020); Trong *et al.* (2021); Hung *et al.* (2022) and this study.

K-feldspar, and quartz, which are similar to those observed in thin sections (Supp Table s1). On Harker diagrams, the compositional variation of the I- and S-type granite shows different trends (Supp Figure S1 (j-r)). While the  $Al_2O_3$ , MnO, and MgO contents from both the I-type granite (Ben Giang-Que Son Permian granitoid) and S-type granite (Hai Van Triassic two-mica granite) are negatively correlated to the  $SiO_2$  contents, the  $TiO_2$ ,  $Fe_2O_3$ , CaO, and  $P_2O_5$  contents of I-type granites are negatively related to the  $SiO_2$  contents. The  $Na_2O$  and  $K_2O$  compositions of the I- and S-type granites are nearly invariable.

The A/CNK ratios for the granitoids range from 0.88 to 1.26, and cluster at the peraluminous and metaluminous domains (Figure 4(f)). The  $K_2O$  contents (1.72 to 4.03 wt

%) were plotted in the medium-high potassium domain (Figure 4(g)). According to the petrographic classification diagrams, most of the granitoid samples were plotted in I-type granite (Ben Giang-Que Son Permian granitoid) and S-type granite (Hai Van Triassic two-mica granite) domains (Figure 4(h)). The compositions of the Permian-Triassic I- and S-type granitoids in this study (Supp Figure S1 and Figure 4) are respectively comparable to those from I- and S-type granite in the Kontum massif (Hoa *et al.* 2008a; Liu *et al.* 2012; Shi *et al.* 2015; Hieu *et al.* 2015, 2017; Qian *et al.* 2019; Thanh *et al.* 2019).

The  $\Sigma REE$  from Permian-Triassic granitoids varies in the range of 94.59–156.29 ppm. The  $\Sigma LREE$  varies from 83.70 to 146.15 ppm, while the  $\Sigma HREE$  ranges from 5.84 to 15.61 ppm (Supp. Table 2). Chondrite-normalized REE

patterns reflect strongly heterogeneous Eu anomalies ( $\text{Eu}/\text{Eu}^* = 0.58\text{--}1.25$ ; Figure 5(d)). Primitive mantle-normalized REE patterns show positive anomalies of Cs, U, K, Pb, and Nd, and negative anomalies of Ba, Nb, Ce, P, Zr and Ti (Figure 5(e,f)). The negative anomalies of Eu and Ba in Permian-Triassic granitoids, similar to those in Ordovician-Silurian granitoids, are possibly caused by the fractionation of the plagioclase and K-feldspar crystallization. The estimated temperature of zircon crystallization calculated using (Watson and Harrison 1983) formula for the Permian-Triassic granitoids varies in the range of  $692.02\text{--}855.81^\circ\text{C}$  (Figure 6(d)). Permian-Triassic granitoids tend to indicate an I-type granite. However, the trend is not obvious. On the tectonic classification diagrams from (Pearce *et al.* 1984), the granitoid of the study area is commonly plotted in collision and subduction zones (Figure 6(e,f)). The trace element composition of granitoids from the study area (Figures 5 and 6) is comparable with that of the granites in the Kontum massif and Song Ma suture zone.

#### 4.2. U-Pb zircon geochronology and Hf isotopic composition

The LA ICP-MS U-Pb zircon dating results for five granitoid samples in this study are shown in Supp Table 3. The ages of rocks are calculated from the average age of the youngest zircon population with individual discordant values  $< 10\%$ . The  $^{206}\text{Pb}/^{238}\text{U}$  ages are used for zircon aged  $< 1000$  Ma, while error margins are given as  $1\sigma$ . The representative cathodoluminescence (CL) images of zircon from five samples (AL08, AL12, AL02, AL17, and AL14) are shown in Supp Figure S2.

Sample AL08 from Dien Binh complex was collected at coordinates  $16^\circ 21' 34.0''\text{N}$  and  $107^\circ 09' 05.2''\text{E}$ . Zircon from this sample in CL images shows a light yellow colour and subhedral-anhedral crystals of short prismatic shape with clear growth zones, which are indicative of a magmatic-sourced zircon (Supp Figure S2(a)). The Th/U ratios for zircon are  $> 0.1$  (i.e.  $1.12\text{--}2.14$ ) and comparable to those from magmatic zircon (Hoskin and Schaltegger 2003). The ages for 30 analyses from sample AL08 vary from 424 Ma to 512 Ma. The youngest concordant zircon population has a weighted mean age of  $452.3 \pm 2.9$  Ma ( $n = 16$ , MSWD = 0.62) and is considered the crystallization age of the granite (Figure 7(a)).

Sample AL12 from Dien Binh complex was collected at coordinates of  $16^\circ 33' 40.8''\text{N}$  and  $106^\circ 57' 24.5''\text{E}$ . Zircon in this sample has a light yellow colour and short prismatic crystals with clear growth zones which is typically observed in magmatic zircon (Supp Figure S2(b)). The outmost metamorphic zones were observed in some

zircon grains. The Th/U ratio from zircon in this sample varies between 0.47 and 2.46, which is  $> 0.1$  and consistent with those from magmatic zircon (Hoskin and Schaltegger 2003). The youngest weighted mean age for 35 zircon grains of sample AL12 was  $448.7 \pm 3.2$  Ma ( $n = 14$ , MSWD = 0.66; Figure 7(b)), which indicates the magma crystallization age. A single inherited zircon age of 776 Ma indicates evidence of an ancient crustal source. The two ages of 366 Ma and 340 Ma were obtained from the outmost metamorphic zones of zircon, indicating post-magmatic tectonothermal episodes. The Devonian timing of later stage magmatism or metamorphic overprint in the metamorphic rim of zircon was recorded in previous documents (Shi *et al.* 2015). However, Devonian magmatic or metamorphic events have never been published in this region.

Sample AL02 from Ben Giang-Que Son complex was collected at coordinates  $16^\circ 14' 50.5''\text{N}$  and  $107^\circ 17' 19.7''\text{E}$ . Zircon grains are pale yellow and commonly have a short prismatic shape with clear growth zones of magmatic zircon (Supp Figure S2(c)). Th/U ratio in zircon, ranging from 0.74 to 2.37, is similar to that from the magmatic zircon (Hoskin and Schaltegger 2003). The  $^{206}\text{Pb}/^{238}\text{U}$  ages obtained from 35 analyses for this sample vary from 242 Ma to 268 Ma, and the weighted mean age for the concordant zircons is  $255 \pm 1.5$  Ma ( $n = 22$ , MSWD = 1.09; Figure 7(c)), which is considered to be the age of magma crystallization.

The sample AL17 from Ben Giang-Que Son complex was collected in the central study area, at the coordinates of  $16^\circ 24' 34.2''\text{N}$  and  $107^\circ 28' 20.5''\text{E}$ . Zircon grains from this sample have a pale yellow colour and needle shape with clear growth zones that are indicative of magmatic zircon. (Supp Figure S2(d)). The Th/U ratio of zircon is  $> 0.1$  (i.e.  $0.81\text{--}2.01$ ) and is consistent with the magmatic zircon morphologies (Hoskin and Schaltegger 2003). The  $^{206}\text{Pb}/^{238}\text{U}$  age from 32 analyses ranges between 248 Ma and 268 Ma and the weighted mean age for the concordant zircons is  $259.3 \pm 3.7$  Ma ( $n = 15$ , MSWD = 0.72; Figure 7(d)) which is believed to be the age of magma crystallization.

The sample AL14 from Hai Van complex was collected in the northern study area, at the coordinates of  $16^\circ 39' 20.2''\text{N}$  and  $106^\circ 49' 00.4''\text{E}$ . Zircon from this sample has a light yellow colour and common needle shape with clear growth zones, which is typically observed in magmatic-sourced zircon (Supp Figure S2(e)). The Th/U ratio of zircon is  $> 0.1$  (i.e.  $0.59\text{--}3.87$ ) and consistent with that from the magmatic zircon (Hoskin and Schaltegger 2003). The youngest population of the (near-) concordant zircons from 24 analyses for sample AL14 is  $243.2 \pm 2.1$  Ma ( $n = 9$ , MSWD = 0.29

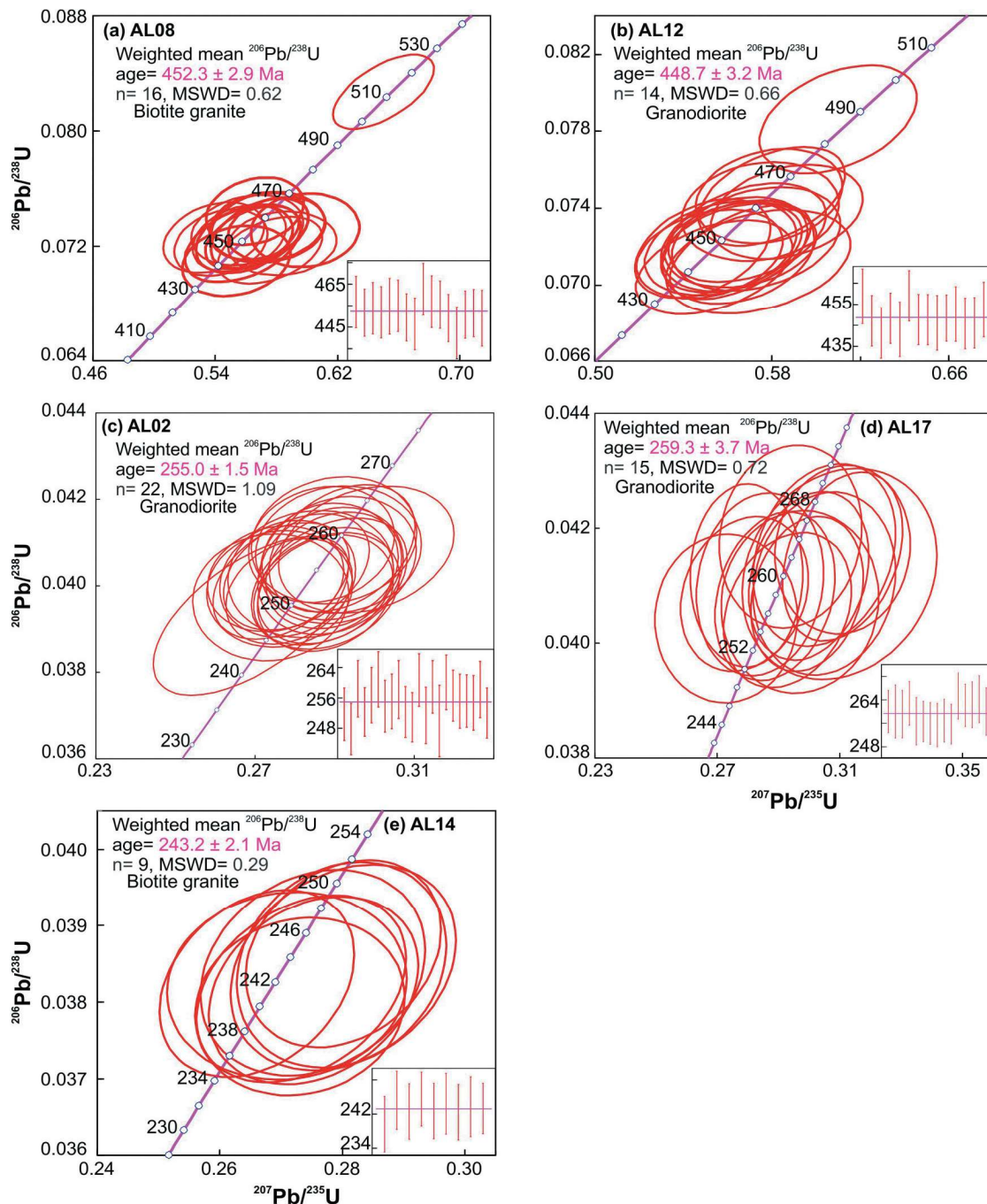


**Figure 7.** LA ICP-MS U-Pb Zircon concordia diagram and weighted mean ages for five granitoid samples from the Dakrong-A Luoi plutonic rocks in the South Truong Son belt.

Figure 7(e) which is considered the magma crystallization age. Inherited ages obtained from the remnant cores of two zircon grains are 874 Ma and 570 Ma which indicate sources of Neoproterozoic continents in the study region.

Twenty zircon grains from sample AL12, twenty zircon grains from sample AL17, and twenty-two zircon grains from AL14 of Dakrong-Aluoi areas were analysed for in situ zircon Hf isotopes, and the obtained results are presented in Supp Table 3.

Twenty zircon grains from sample AL12 exhibit the measured  $^{176}\text{Lu}/^{177}\text{Hf}$  and  $^{176}\text{Hf}/^{177}\text{Hf}$  ratios of 0.000399 to 0.001618 and 0.282670 to 0.282738, respectively. They indicate a narrow range of  $\square_{\text{Hf}}$  ( $t = 452$  Ma) values from +6.2 to +8.3 (Supp Table 3), with a weighted average value of  $7.5 \pm 1.1$  (MSWD = 0.06,  $n = 20$ ) (Figure 8(a)). The  $T_{\text{DM1}}$  ages range from 738 to 818 Ma and  $T_{\text{DM2}}$  ages from 907 to 1046 Ma (Supp Table 3), with a weighted average  $T_{\text{DM2}}$  age of  $962 \pm 19$  Ma (MSWD = 2.5,  $n = 20$ ) (Figure 8(b)).

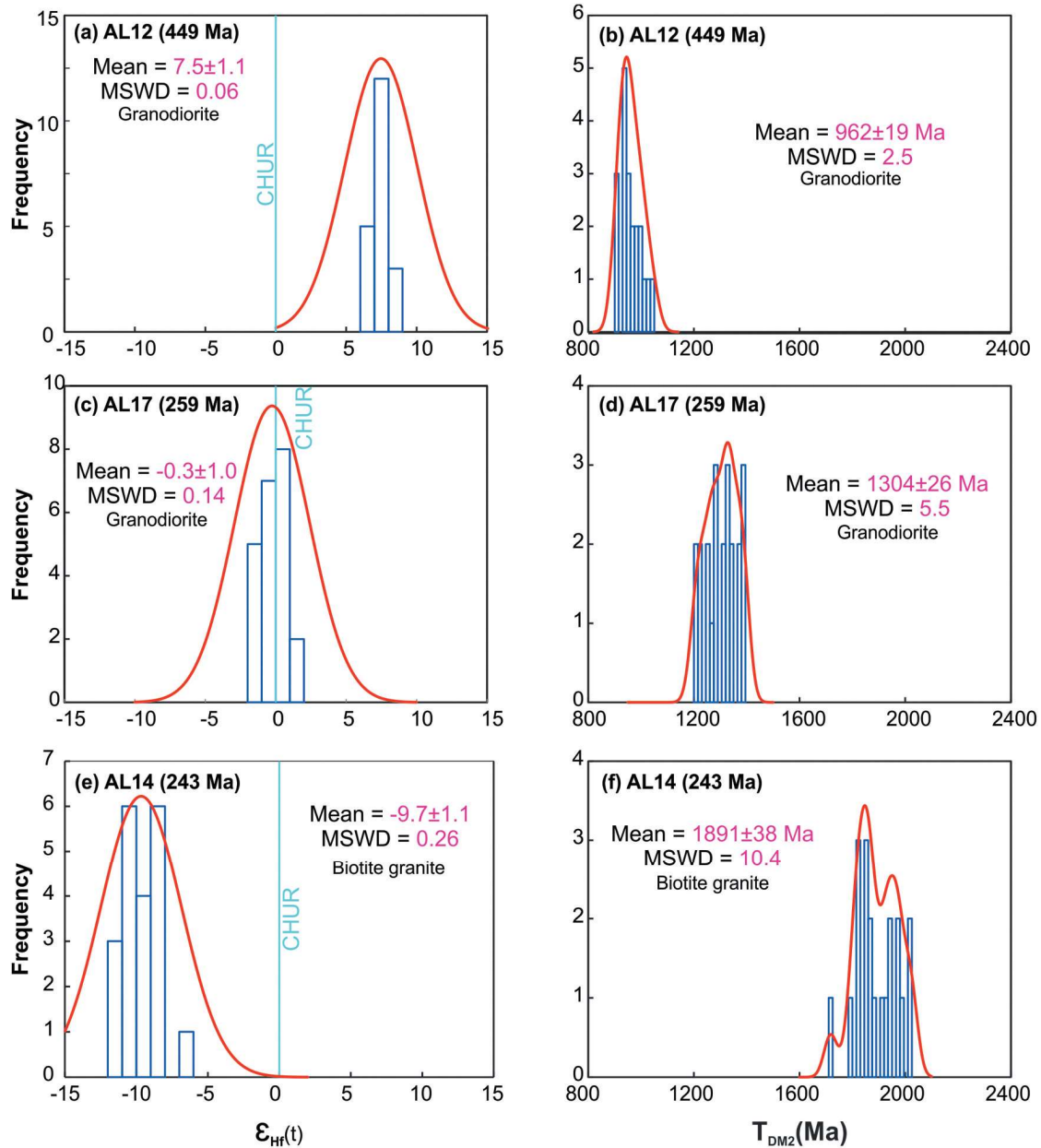


**Figure 8.** Initial  $\epsilon_{\text{Hf}}$  values and Hf model zircon ages for three magmatic events (AL08: 454 Ma; AL17: 261 Ma; and AL14: 246 Ma) in the Dakrong-A Luoi, south truong son belt.

Twenty zircon grains from sample AL17 exhibit the measured  $^{176}\text{Lu}/^{177}\text{Hf}$  and  $^{176}\text{Hf}/^{177}\text{Hf}$  ratios of 0.000548 to 0.006194 and 0.282571 to 0.282678, respectively. They indicate a narrow range of  $\epsilon_{\text{Hf}}$  ( $t = 259$  Ma) values from  $-1.6$  to  $+1.3$  (Supp Table 3), with a weighted average value of  $-0.3 \pm 1.0$  (MSWD = 0.14,  $n = 20$ ) (Figure 8(c)). The  $T_{\text{DM1}}$  ages range from 875 to 991 Ma and  $T_{\text{DM2}}$  ages from 1205 to 1390 Ma (Supp Table 3), with a weighted average  $T_{\text{DM2}}$  age of  $1304 \pm 26$  Ma (MSWD = 5.5,  $n = 20$ ) (Figure 8(d)).

Twenty-two zircon grains from sample AL14 exhibit the measured  $^{176}\text{Lu}/^{177}\text{Hf}$  and  $^{176}\text{Hf}/^{177}\text{Hf}$  ratios of 0.000366 to 0.002280 and 0.282291 to 0.282430, respectively. They indicate a narrow range of  $\epsilon_{\text{Hf}}$  ( $t = 243$  Ma) values from  $-11.9$  to  $-7.0$  (Supp Table 3), with a weighted average value of  $-9.7 \pm 1.0$  (MSWD = 0.26,  $n = 22$ ) (Figure 8(e)). The  $T_{\text{DM1}}$  ages range from 1183 to 1350 Ma and  $T_{\text{DM2}}$  ages from 1721 to 2028 Ma (Supp Table 8), with a weighted average  $T_{\text{DM2}}$  age of  $1891 \pm 38$  Ma (MSWD = 10.4,  $n = 22$ ) (Figure 8(f)).

## 5. Discussion

### 5.1. Ordovician-Silurian and Permian-Triassic granitoids magmatism in Dakrong-A Luoi area, Truong Son belt

The LA ICP-MS U-Pb zircon dating results of magmatic formations in the Dakrong-A Luoi area of the Truong Son belt in central Vietnam in this study have recorded at least three magmatic events in the area, from the Paleozoic to the Mesozoic.

The first magmatic event is marked by ~452 Ma granitoids (Figure 7(a,b); Supp Table 3) intruded into Early Paleozoic sequences, and were occasionally overlain by Jurassic sediments (Figure 1(b)). This Ordovician granitoid has similar geochemical and mineralogical composition to those from the coeval I-type granites in the Kontum massif, south of the Truong Son belt (i.e. Dien Binh granodiorite and Tra Bong granitoid; Trong *et al.* 2021; Ngo *et al.* 2023) and 460 Ma granitoid (LA-ICPMS zircon age) in northern Laos, western Indochina block (Wang *et al.* 2020). The granitoid age in this study is consistent with those of Kontum massif, and quite similar to those of the Cathaysia block. The Yangtze block concentrates mostly in the 430–410 Ma age range, with a few samples reaching as far as 470 Ma; this age range is distinct from that of the Kontum massif and the study area (Figure 10(a)).

The second magmatic event has been recorded by the Late Permian granitoids aged 259–255 Ma (Supp Table s3; Supp Figure s2(c,d) and Figure s7(c,d)) intruded into Paleozoic Sequences. These magmatic rocks have similar mineralogy and geochemical patterns to those recorded in the coeval I-type granite from the Ben Giang-Que Son complex in the Kontum massif (Sang 2011; Minh *et al.* 2022), and the coeval I-type granite in the Song Ma suture zone, northwest Vietnam (Liu *et al.* 2012; Hieu *et al.* 2017).

The third magmatic event is recorded by the widespread Middle Triassic granitoids aged 243 Ma (Supp Table 3; Supp Figure s2(e) and Figure s7(e)) intruded into Paleozoic Sequences (Figure 1(b)) and locally contain xenolith of Proterozoic metamorphic-sedimentary rocks (Hieu *et al.* 2015; Thanh *et al.* 2019). These Middle Triassic S-type granite formations are widely recorded in the Song Ma suture zone, such as Phia Bioc and Muong Lat granites (Hieu *et al.* 2017; Thanh *et al.* 2019).

In the Permian-Triassic period, the granitoids in this study are synchronous with granitic emplacements of the Kontum massif, northwest Vietnam and Cathaysia (270–240 Ma), South China block, but older than the Yangtze (225–210 Ma), South China block (Figure 14 (c,d)).

## 5.2. Petrogenesis

### 5.2.1 Petrogenesis of Ordovician-Silurian granitoids

The Ordovician-Silurian granitoids in the study area have a mineral composition of plagioclase, K-feldspar quartz, hornblende, and biotite, and geochemical composition of 63.77–70.76 wt% SiO<sub>2</sub> and 13.86–16.73 wt% Al<sub>2</sub>O<sub>3</sub>. These composition characteristics indicate that they are quartz diorite and I-type granite. On the lithological classification diagram of Pearce (1983); Pearce *et al.* (1984), the granitoids were mainly plotted in the domains of volcanic arc granites (the VAG) and syn-collision granites (syn-COLG) (Figure 6(b)). The estimated temperature formation for the Ordovician-Silurian granitoids calculated based on (Watson and Harrison 1983) zircon thermometer ranges from 750°C to 850°C (Figure 6(a)). The Ordovician-Silurian granitoid in the Dakrong-Aluoi area, with all characteristics above compared to the magmatism and tectonic history of the region, is considered to have been formed at a volcanic arc margin during the Early Paleozoic, coeval with the Paleozoic granitoid in the Kontum massif (Figure 6(a–c), Supp Table 5). Notably, the coeval extrusive rock of the Ordovician-Silurian magmatism in both Dakrong-A Luoi and Kontum massif areas has not been recorded (Trong *et al.* 2021).

Isotopic data show compositional ranges of zircon  $\epsilon_{\text{Hf}}$  (t) from +6.2 to +8.3, and zircon Hf model ages ( $T_{\text{DM2}}$ ) from 907 to 1046 Ma (Figures 9 and 10, Supp Table 7). These isotopic characteristics suggest that the Ordovician-Silurian granitoids were derived from the partial melting of mantle material with an amount of crustal source. The  $\epsilon_{\text{Hf}}$ (t) and zircon Hf model ages ( $T_{\text{DM2}}$ ) of the study area match well with I-type granite in the Kontum massif area and are different from S-type granite in the Kontum massif (Figure 9(a–f)). The Hf isotopic composition of the Ordovician-Silurian granitoid (i.e.  $\epsilon_{\text{Hf}}$ (t) = +6.2 to +8.3) is similar to the isotopic composition reported for the +6.2 to +8.3 Ben Giang granitoids in the Kontum basement (i.e.  $\epsilon_{\text{Nd}}$ (t) = +6.2 to +10) (Trong *et al.* 2021), Cathaysia and Yangtze, South China (Figure 10(a,b)).

### 5.2.2 Petrogenesis of Permian-Triassic granitoids

The results from this study have confirmed the formation of Permian-Triassic I-type and S-type granites in the Dakrong-Aluoi area. The I-type granites are characterized by hydrous minerals such as hornblende and biotite and do not contain aluminium-rich minerals such as muscovite and cordierite (Figure 3(c–f)). In the field, this rock type does not contain xenolith. In terms of geochemical patterns, I-type granite has low SiO<sub>2</sub> (61.80–66.75%) and high Fe<sub>2</sub>O<sub>3</sub> and MgO, and was

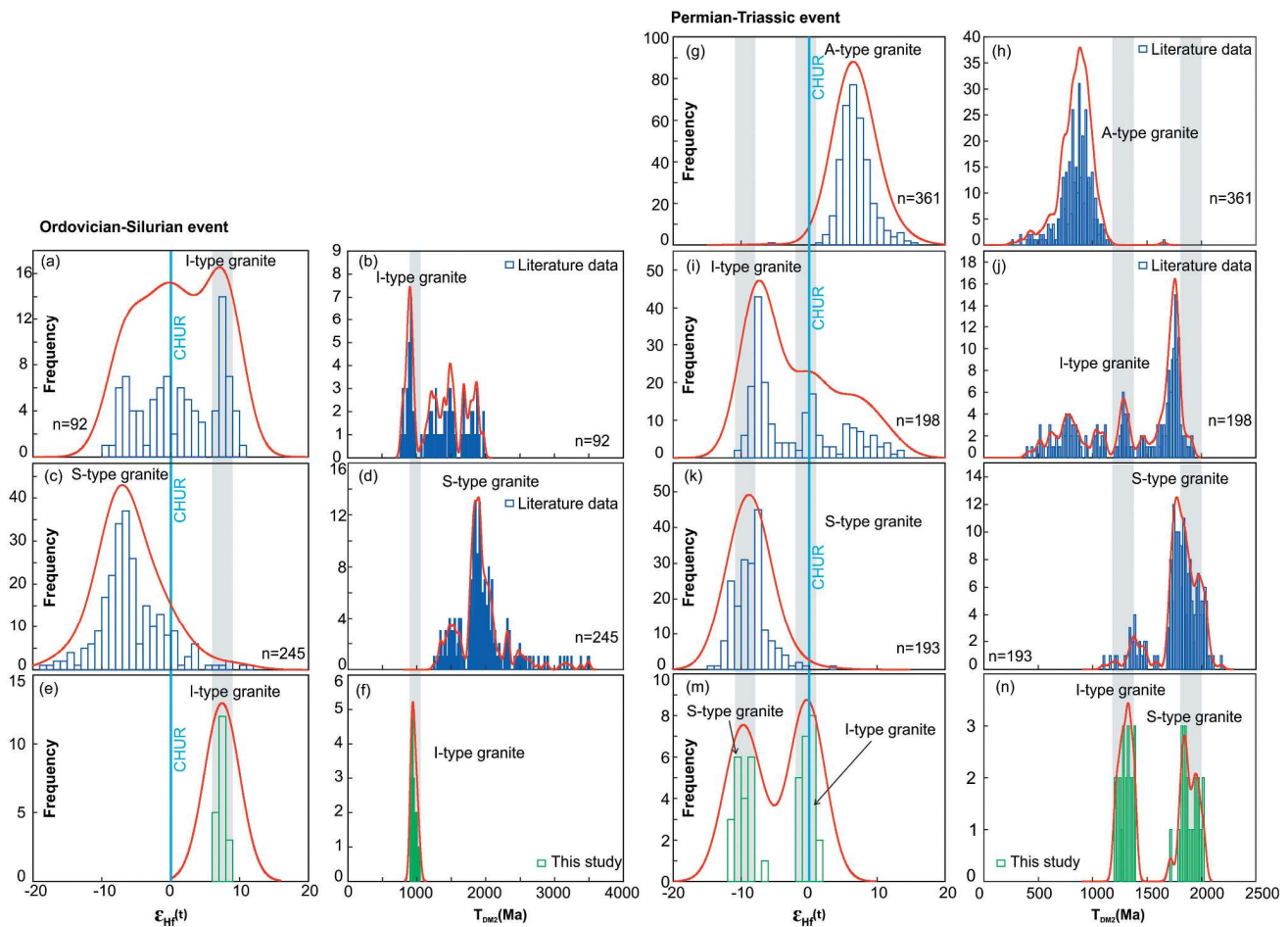


**Figure 9.** Initial  $\epsilon_{\text{Hf}}$  values and Hf model zircon ages from this study and the Indochina block. Literature data is derived from Hieu *et al.* (2013) (Hieu *et al.* 2015); (Hieu *et al.* 2016) (Hieu *et al.* 2017); (Hieu *et al.* 2020); Usuki *et al.* (2015); Wang *et al.* (2016); Minh *et al.* (2018); Thanh *et al.* (2019); Qian *et al.* (2019); Minh *et al.* (2020); Jiang *et al.* (2020); Trong *et al.* (2021); Minh *et al.* (2022); Hung *et al.* (2022); Hoang *et al.* (2023) and this study.

plotted in the metaluminous series with an average A/CNK value of 0.93 (Figure 4(e,f)). On the  $\text{SiO}_2\text{-P}_2\text{O}_5$  diagram, the I-type granites were plotted in form of the I-type trends (Supp Figure s1(r)). In the chondrite and primitive normalization schemes (Figure 5(d–f)), the I-type granites demonstrate enrichment in Cs, U, Pb and Nd and depletion in Ba, Nb, Ta, P, Eu and Ti, corresponding to the fractional crystallization of common minerals (e.g. K-feldspar, apatite, and biotite). The zircon thermometer using (Watson and Harrison 1983) formula exhibits that I-type granites were formed at 692°C–732°C (Supp Table s1 and Figure 6(d)).

Compared to the regional tectonic history, these rocks were formed in a volcanic arc terrane (Figure 6(e,f)) developed by the amalgamation of Indochina and South China blocks. Notably, no remnant core in zircon grains as well as no inherited age have been recorded in the Permian-Triassic I-type granitoid samples, while the zircon  $\epsilon_{\text{Hf}}$ (t) values range from –1.60 to 1.32, and Hf isotopic model ages

( $T_{\text{DM}2}$ ) of 1205–1390 Ma (Figure 8(c,d)). These characteristics suggest that the I-type granites were likely produced from partial melting of Mesoproterozoic continental crust with a small contribution of mantle-derived components (Figure 8(d)). Compared to the ancient Kontum basement, the  $\epsilon_{\text{Hf}}$ (t) of I-type granites are close to the Cha Val granitoid (i.e.  $\epsilon_{\text{Hf}}$ (t) = –1.04 to 2.71), suggesting that their origins are close together (Figure 9).

The 246 Ma S-type granites in the Dakrong-Aluoi area, at the field, intruded into the 261 Ma granodiorite. The S-type granites commonly contain xenoliths of two-mica quartz and schists. Geochemically, they are characterized by high  $\text{SiO}_2$ ,  $\text{Al}_2\text{O}_3$  and total alkalinity ( $\text{K}_2\text{O}+\text{Na}_2\text{O}$ ) but low  $\text{TiO}_2$ , MgO, and A/CNK ratio (1.01–1.26) that are typical characteristic of the S-type type granite. The geochemical patterns of these granites (Supp. Table 6 and Figures 4–6) are consistent with those from the S-type granites in the Kontum massif (i.e. Muong Lat granite, Phia Bioc granite in the Song Ma suture zone



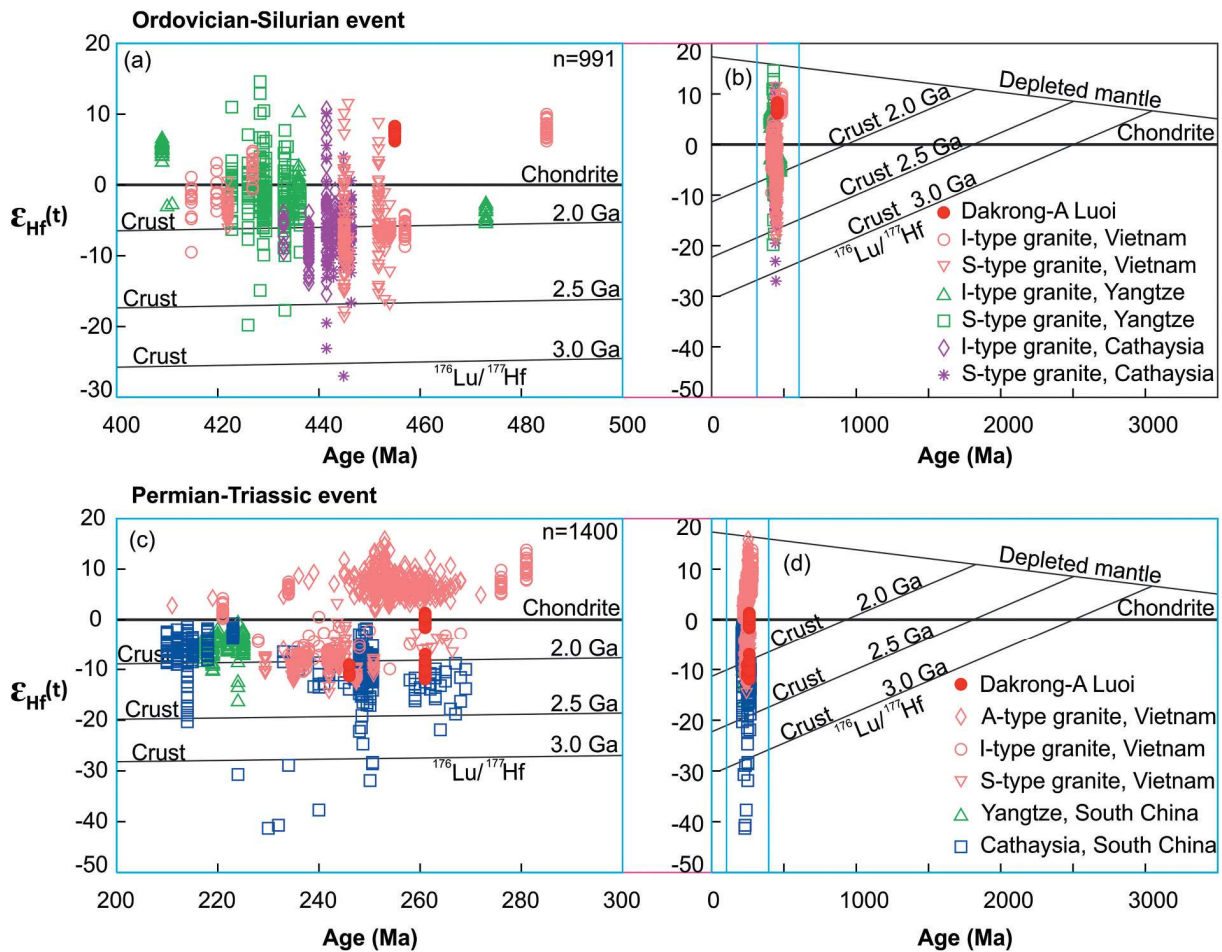


**Figure 10.** Initial  $\epsilon_{\text{Hf}}$  values and Hf model zircon ages from the this study, Vietnam, Cathaysia and Yangtze. Literature data is derived from Chu *et al.* (2012); Zhong *et al.* (2013); Hieu *et al.* (2013) (Hieu *et al.* 2015); (Hieu *et al.* 2016) (Hieu *et al.* 2017); (Hieu *et al.* 2020); Usuki *et al.* (2015); Fu *et al.* (2015); Jiao *et al.* (2015); Wang *et al.* (2016); Yu *et al.* (2016); Li *et al.* (2016); Zhou *et al.* (2017); Gao *et al.* (2017); Minh *et al.* (2018); Xu *et al.* (2018); Thanh *et al.* (2019); Qian *et al.* (2019); Minh *et al.* (2020); Jiang *et al.* (2020); Liu *et al.* (2020); Trong *et al.* (2021); Minh *et al.* (2022); Hung *et al.* (2022); Song and Xu (2022); Hoang *et al.* (2023); Xiao *et al.* (2023) and this study.

and Hai Van granite; Hieu *et al.* 2015, 2017, 2020; Shi *et al.* 2015; Thanh *et al.* 2019). The S-type granites in the study area have low  $\epsilon_{\text{Hf}}$ (t) value (−11.9 to −7.0) and Hf isotopic model ages ( $T_{\text{DM}2}$ ) (1.7 to 2.0 Ga) indicating that this S-type granite was derived from the partial melting of the Paleoproterozoic continental crust. The  $\epsilon_{\text{Hf}}$ (t) and zircon Hf model ages ( $T_{\text{DM}2}$ ) of I-type and S-type granites in the study area are similar to those of the I-type and S-type granites in the Kontum massif, north Truong Son belt, and northwest Vietnam, and distinct from the A-type granite in the northwest region of Vietnam (Figure 9(g–n), Supp Table 8).

### 5.3. Paleozoic-Mesozoic granitoid evolution in the study area

The Indochina block which was derived from the north coast of Gondwanaland, is the largest structure of mainland Southeast Asia (Figure 1(a)) (Metcalf 2006; Roger

*et al.* 2007).; The Indochina block in Vietnam is composed of three main units, including the Truong Son belt in the north, the Kontum massif in the centre and the Dalat zone in the south. The Dakrong-A Luoi area is the farthest southern region of the Truong Son belt, adjacent to the Kontum massif. The boundary between the Truong Son belt and the Kontum massif is defined by the TKPS suture (Figure 1(b)). Lepvrier *et al.* (2008) indicate that the Truong Son belt and the Kontum massif, since being drifted from the Gondwana margin, have been considered the same geological terrane throughout the Paleozoic-Mesozoic tectonic events including subduction, collision and extension.

Ordovician-Silurian metamorphic-magmatic activities in the Truong Son belt and Kontum massif, as in recent publications, are recorded by 407–490 Ma igneous rocks in the Truong Son belt (Tran *et al.* 2014; Shi *et al.* 2015; Gardner *et al.* 2017; Jiang *et al.* 2023; this study) and 403–482 Ma magmatic rocks in the Kontum massif

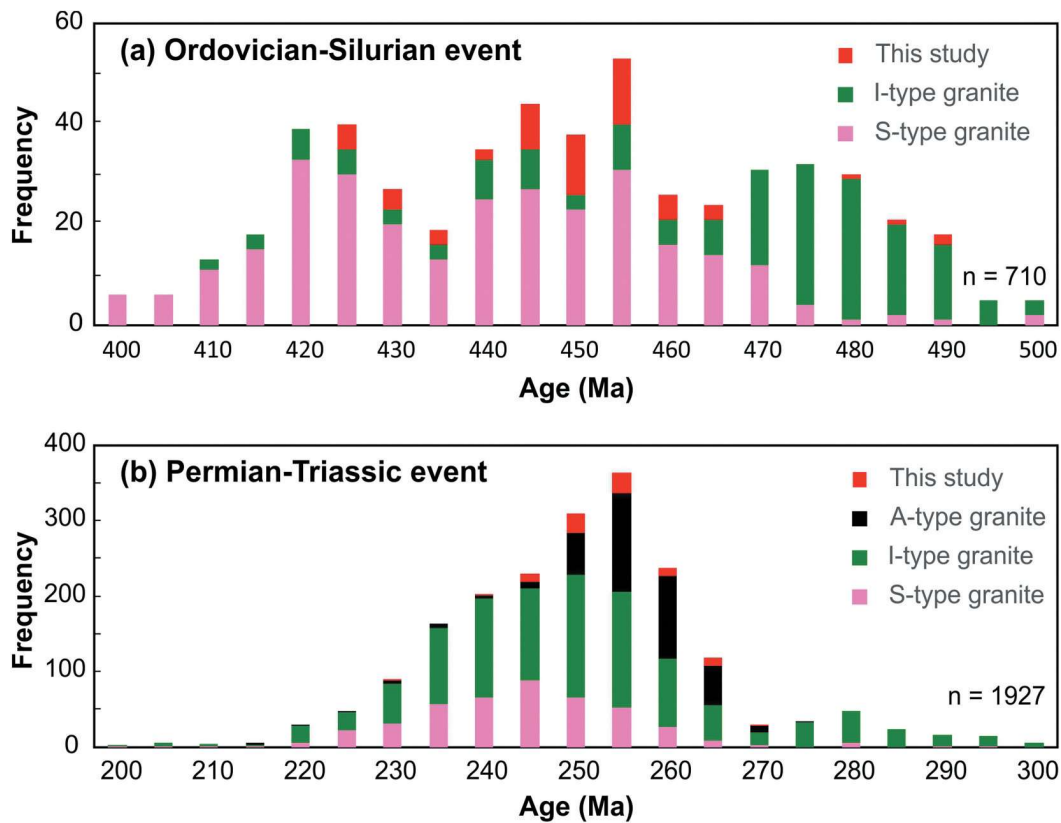


**Figure 11.** The classification of I-, S- and A-type granite from this study, Vietnam and north Laos in the Indochina.

(Figure 11(a)) (Carter *et al.* 2001; Nagy *et al.* 2001; Maluski *et al.* 2005; Roger *et al.* 2007; Usuki *et al.* 2009; Minh *et al.* 2020; Jiang *et al.* 2020; Trong *et al.* 2021; Nakano *et al.* 2021); Shi *et al.* (2015) proposed four main magmatic events occurred during the Paleozoic-Mesozoic at the Truong Son belt: the Ordovician-Silurian (420–470 Ma), Early Carboniferous-Permian (280–300 Ma), Late Permian to Middle Triassic (245–270 Ma) and the Middle-Late Triassic (200–245 Ma) (Figure 11(b)).

The ages of Ordovician-Silurian granite of the I-type granite in the Indochina block vary from 500 Ma to 410 Ma, largely concentrated 490–455 Ma, and the ages of the S-type granite range from 500 Ma to 400 Ma, mainly concentrated 460–420 Ma (Figures 11(a) and Supp Table 9). The Ordovician-Silurian magmatic event is understood as being formed during the bilateral subduction of the TKPS ocean, in which the ocean moved beneath the Kontum massif to the south and moved beneath the Truong Son belt to the north (Gardner *et al.* 2017; Jiang *et al.* 2023). As shown in Figure 14, during this time period, the values of  $\varepsilon_{\text{Hf}} = -9.5$  to  $+10.0$  and  $T_{\text{DM2}} = 692$  Ma to  $1421$  Ma ( $\varepsilon_{\text{Hf}} = +6.2$  to  $+10.0$  and  $T_{\text{DM2}} = 692$  Ma to  $841$  Ma from Ben Giang granitoid;  $\varepsilon_{\text{Hf}} = -8.7$  to  $-4.2$  and  $T_{\text{DM2}} = 1237$  Ma to  $1421$  Ma from Dien Binh granitoid; and  $\varepsilon_{\text{Hf}} = -9.5$  to  $+4.8$  and  $T_{\text{DM2}} = 896$  Ma to  $1393$  Ma from Dai Loc granitoid) in the southwestern subduction direction exhibited

a significantly wider range than the value of  $\varepsilon_{\text{Hf}} = +6.2$  to  $+8.3$  and  $T_{\text{DM2}} = 737$  Ma to  $817$  Ma ( $\varepsilon_{\text{Hf}} = +6.2$  to  $+8.3$  and  $T_{\text{DM2}} = 737$  Ma to  $817$  Ma from Dakrong-A Luoi granitoid) in the northeast subduction direction. Therefore, the origin of the materials that create the rocks between bilateral subduction is different in certain ways, particularly on the southwest subduction direction, which is where S-type granite is typically formed. Paleo Tethys oceanic crust in the central beneath the bilateral subduction consequently and the 490–450 Ma arc magmatic rocks were formed in SW Kontum massif and NE Truong Son belt (i.e. Dien Binh, Dak To, Donken and Ben Giang granites; Figure 14(a,b)). During 450–430 Ma, the amalgamation of the Truong Son belt and Kontum massif occurred along the TKPS suture zone, forming the S-type Dai Loc and Chu Lai granites (Minh *et al.* 2020; Jiang *et al.* 2020), pegmatite, and metamorphic rocks of amphibolites and gneiss (Usuki *et al.* 2009; Cuong *et al.* 2021; Nam *et al.* 2003; Figures 11(a) and 14(a,b), Supp Table 9). This study's results, together with those from Gardner *et al.* (2017) for Ordovician-Silurian dioritic pluton and tuff rhyolite mapped in the Donken area, Southeast Laos, have added strong evidence for a comprehensive understanding of the bilateral subduction event, with additional evidence of coeval subduction of the TKPS ocean beneath the Truong Son belt (Figure 14(a); Supp Table 5).

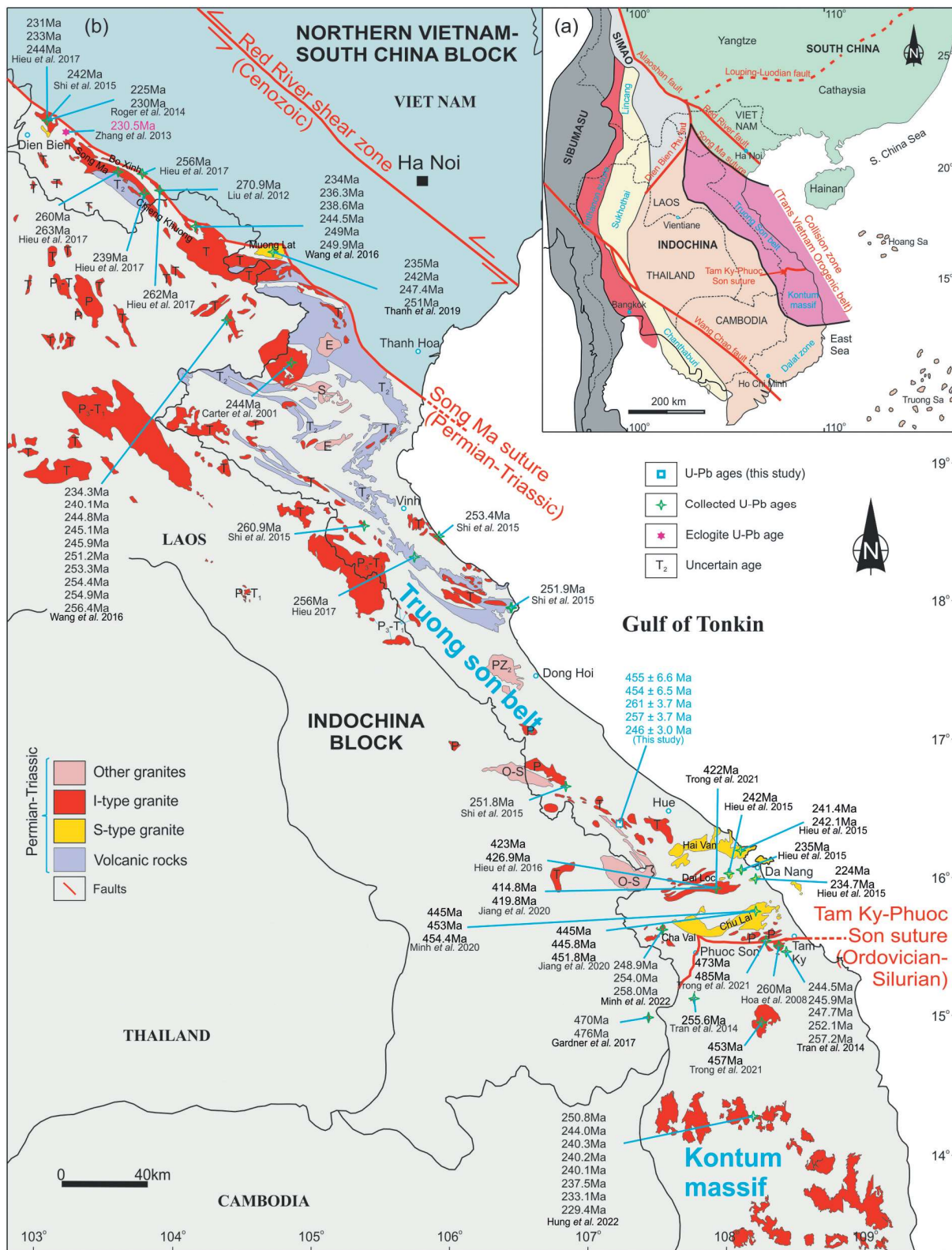


**Figure 12.** (a) Tectonic sketch for the central and eastern Asia and (b) simplified geological map of the Indochina block showing emplacement ages of Permian-Triassic magmatic rocks (geochronological data sources: this study; Carter *et al.* 2001; Hoa *et al.* 2008a; Liu *et al.* 2012; Żelaźniewicz *et al.* 2013; Hieu *et al.* 2013, 2015, 2017; Zhang *et al.* 2013; Tran *et al.* 2014; Roger *et al.* 2014; Shi *et al.* 2015; Wang *et al.* 2016; Minh *et al.* 2018; Thanh *et al.* 2019; Hung *et al.* 2022).

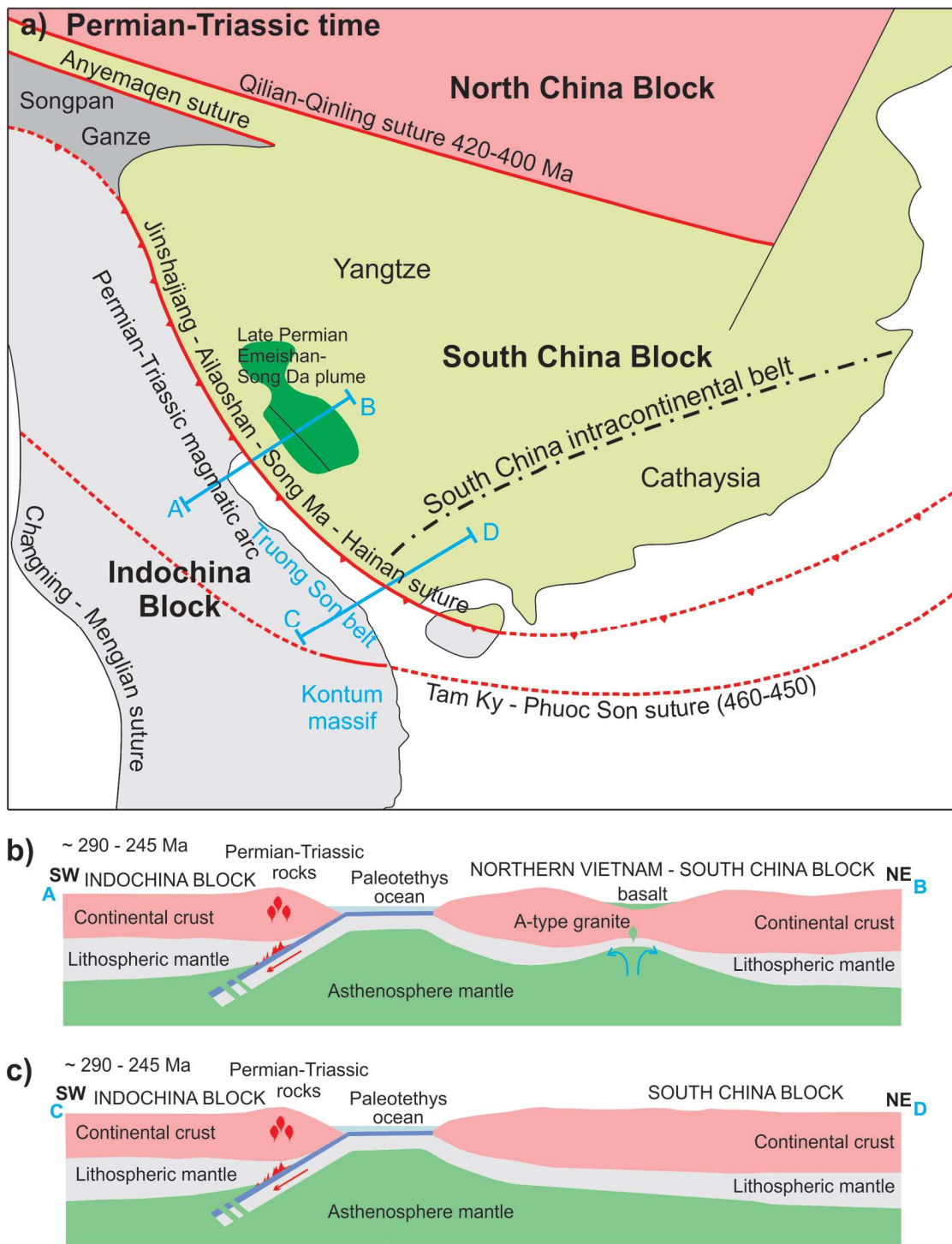


**Figure 13.** (a) Tectonic reconstruction of the Indochina block and nearby blocks in Permian-Triassic from the South China to Indochina. (b,c) Permian-Triassic geodynamic evolution in song ma suture and Truong Son belt during closure of the northern branch of the Palaeo-Tethys Ocean (Faure *et al.* 2018; Minh *et al.* 2022).

Studies on magmatic activity associated with the subduction and closure of the Paleo-Tethys Ocean in Vietnam during the Late Paleozoic-Early Mesozoic have provided essential evidence of these tectonic events (Figures 12 and 13a) (Hoa *et al.* 2008a, 2008b; Liu *et al.* 2012; Żelaźniewicz *et al.* 2013; Hieu *et al.* 2013, 2015,

2017; Shi *et al.* 2015; Thanh *et al.* 2019; Minh *et al.* 2022).; Figure 13(b) shows the widespread distribution of granitic rocks in Vietnam during the Permian-Triassic, which can be respectively correlated to the subduction and collision events in the Truong Son belt and the Kontum massif. The Truong Son belt (Figure 12b) is partially

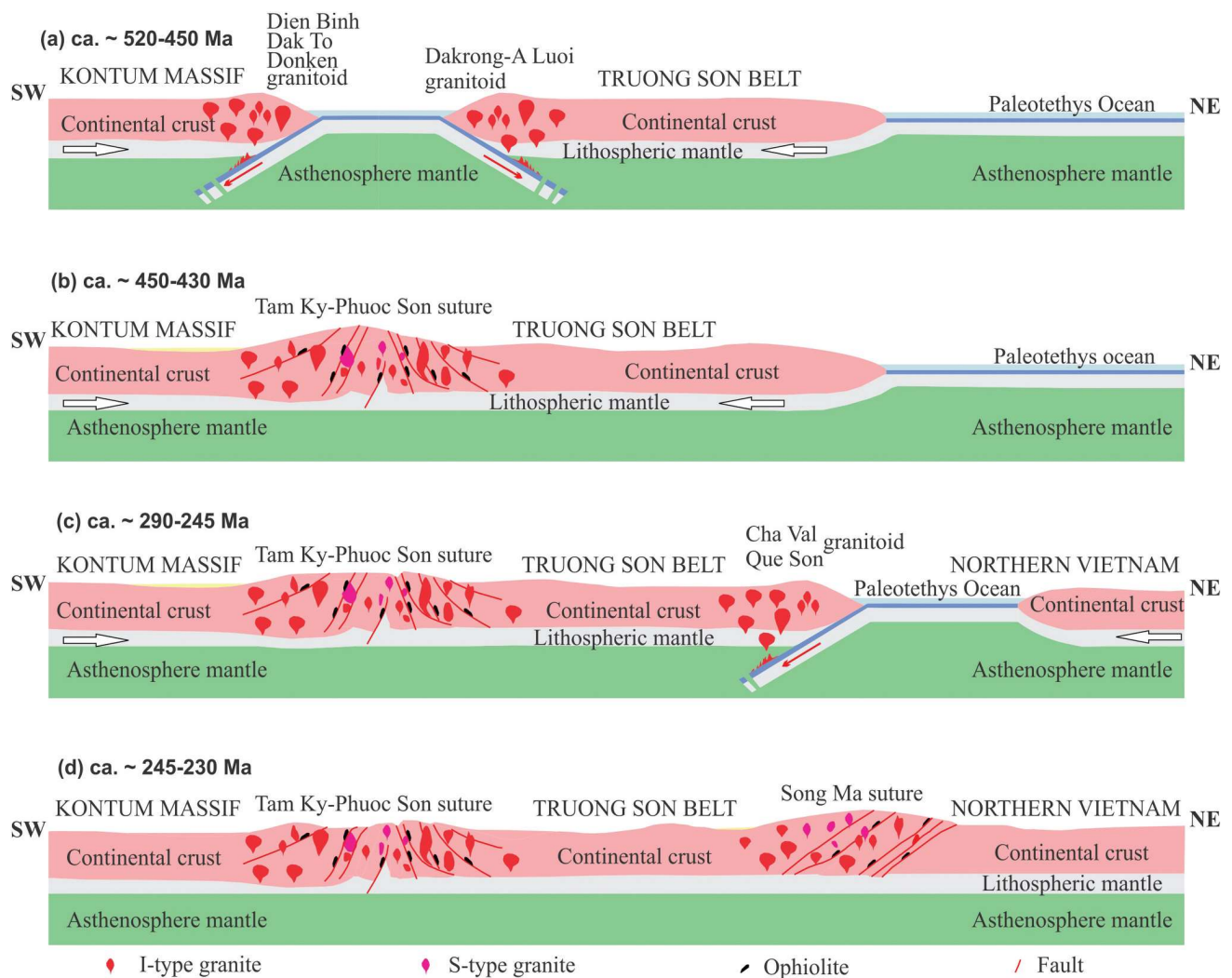


**Figure 14.** Palaeozoic-Mesozoic tectonic-magmatic evolution model of the Truong Son belt (Shi *et al.* 2015; Hieu *et al.* 2015; Gardner *et al.* 2017; Nakano *et al.* 2021). (a) 520–450 ma Cambrian-Ordovician setting during the Tamky-Phuoc Son ocean bidirectional subduction. (b) 450–430 ma Ordovician-Silurian setting accompanied with continent-arc collision. (c) 290–245 ma Permian-Triassic setting accompanied with southwest-dipping subduction of paleotethyan song ma ocean. (d) 245–230 ma Triassic setting related to collision of Northern Vietnam and Truong Son belt.

made up of I-type granites (i.e. Chieng Khuong, Dien Bien and Song Ma granites), which were formed during the subduction of the South China block beneath the Indochina block along the Song Ma suture zone during the Permian-Triassic (Cross section AB, Figure 13(b) (Minh *et al.* 2022).; In the Kontum massif, central Vietnam (Figure 12(b)), Cha Val and Que Son granites were formed during the Permian-Triassic subduction of the Paleo-Tethys ocean beneath the Indochina blocks (Cross section CD, Figure 13(c) (Minh *et al.* 2022).,

In this study, the Late Permian I-type granites are metaluminous and high K and are related to the magmatic activities of Andean continental arc subduction (Figures 3, 4, and 7). The U-Pb zircon age (261–257 Ma) of Dakrong-A Luoi I-type granites in the South Truong Son belt (Figure 6(d–f)) and I-type granites in the

northern area of the Truong Son belt are grouped into The Trans Vietnam orogenic belt (Figure 12(a)) (Osana *et al.* 2008) and are considered as Permian-Triassic magmatic arcs (Figure 12(b)) (Faure *et al.* 2018). They are considered to be a southern part of the Trans Vietnam Orogenic belt located in the Permian-Triassic magmatic arc with the same characteristics of origin and age. The Indochina block has A-type granite with ages ranging from 270 Ma to 215 Ma and I-type granite with ages ranging from 300 Ma to 200 Ma, with a focus on 280–240 Ma (Figures 11(b) and Supp Table 10). The I-type granites in Dakrong-A Luoi area can be formed during the Permian-Triassic (290–245 Ma) subduction of the Paleo-Tethys Ocean beneath the Indochina block along the Song Ma suture zone (Figures 11(b) and 14(c), Supp Table 10).

The Song Ma suture is widely considered the boundary between the Indochina block and the South China block (Hutchison 1989; Findlay and Trinh 1997; Lepvrier *et al.* 1997, 2008; Metcalfe 2013). The presence of Bo Xinh and Nui Nua ultramafic rocks along the Song Ma suture zone is considered an ancient oceanic crust remnant of the Paleo-Tethys Ocean (Thanh *et al.* 2011). Most geologists agree that the collision between the two blocks occurred during the Triassic (e.g. Lepvrier *et al.* 2008; Nakano *et al.* 2008; Faure *et al.* 2014; Hieu *et al.* 2017, 2020; Thanh *et al.* 2019). The Indosinian orogeny during Triassic at the Song Ma suture zone, northern Truong Son belt, was marked by the metamorphic rocks at greenschist-amphibolite facies of the Nam Co formation, the serpentinized peridotites and gabbro, and the formation of the Song Ma, Chieng Khuong and Muong Lat granites (Hieu *et al.* 2017; Hau *et al.* 2018; Thanh *et al.* 2019). The evidence for this tectonic along the Song Ma suture zone includes (1) The  $^{40}\text{Ar}/^{39}\text{Ar}$  ages of 240–260 Ma for amphibolite, biotite and muscovite minerals in the metamorphic rocks of the Nam Co Formation (Lepvrier *et al.* 2004) and (2) SHRIMP LA ICP-MS zircon and monazite ages of 230–243 Ma for eclogite and two-mica and garnet-bearing schists in the Song Ma suture zone (Nakano *et al.* 2010; Zhang *et al.* 2013). The eclogite is evidence for the collision and subduction boundary of the two blocks occurring in the Song Ma suture zone. The ages of the S-type granite in the Indochina block range from 270 Ma to 210 Ma, with an emphasis on 250–240 Ma (Figures 11(b) and Supp Table S10). The 246 Ma granite in this study is S-type granite, which is formed from the partial melting of Paleoproterozoic crust, similar to the origin of the Hai Van and Muong Lat complexes (Hieu *et al.* 2015; Thanh *et al.* 2019), was directly related to the Early Triassic collision between the Indochina and South China blocks. The results of this investigation are congruent with the findings of the previous results from (Faure *et al.* 2014) in which the collision between the Indochina and South China blocks is thought to be the result of the Paleo-Tethys closure during the Middle Triassic (Figure 14(d)).

## 6. Conclusions

Based on the whole-rock geochemistry, zircon U-Pb geochronology, and Lu-Hf isotopic compositions of Paleozoic to Mesozoic rocks in Dakrong-A Luoi zone, central Vietnam, the following conclusions can be reached:

The granitoid magmatic activity in Dakrong-A Luoi zone mainly consists of two periods: Ordovician-Silurian (~452 Ma) and late Permian to early Triassic (259–243 Ma).

Ordovician-Silurian granitoids were derived from the partial melting of mantle material with an amount of crustal source, related to the subduction process of the Tam Ky-Phuoc Son ocean moved beneath the Truong Son belt.

Late Permian to early Triassic granite contains two types of granite: I-type granite and S-type granite. I-type granites were likely produced from the partial melting of Mesoproterozoic continental crust with a small contribution of mantle-derived components and S-type granite was derived from the partial melting of the Paleoproterozoic continental crust, which is related to the Late Permian to early Triassic subduction/collision between the Indochina and South China blocks.

## Acknowledgments

This study was funded by VAST05.02/21–22 and partially by state assignment projects of VAST (NCVCC33–01/22–23). James Cook University, Australia, is gratefully acknowledged for providing zircon U-Pb dating analysis facilities. Thanks are due to Prof. Wang for analytical assistance.

## Disclosure statement

No potential conflict of interest was reported by the author(s).

## Funding

The work was supported by the Vietnam Academy of Science and Technology.

## References

- Bouvier, A., Vervoort, J.D., and Patchett, P.J., 2008, The Lu–hf and Sm–nd isotopic composition of CHUR: Constraints from unequilibrated chondrites and implications for the bulk composition of terrestrial planets: *Earth and Planetary Science Letters*, v. 273, p. 48–57. doi:10.1016/j.epsl.2008.06.010.
- Carter, A., Roques, D., Bristow, C., and Kinny, P., 2001, Understanding Mesozoic accretion in Southeast Asia: Significance of Triassic thermotectonism (indosinian orogeny) in Vietnam: *Geology*, v. 29, p. 211–214. doi:10.1130/0091-7613(2001)029<0211:Umaisa>2.0.Co;2.
- Chu, Y., Lin, W., Faure, M., Wang, Q., and Ji, W., 2012, Phanerozoic tectonothermal events of the Xuefengshan belt, central South China: Implications from U-Pb age and Lu-hf determinations of granites: *Lithos*, v. 150, p. 243–255. doi:10.1016/j.lithos.2012.04.005.
- Cuong, T.C., Hieu, P.T., Minh, P., Kawaguchi, K., Anh, N.T.Q., and HUNG, K.T., 2021, Zircon U–pb ages of the pegmatites in the Kontum massif, central Vietnam and their quality evaluation for ceramic industry: *Journal of Mineralogical and Petrological Sciences*, v. 116, p. 279–292. doi:10.2465/jmps.210911.
- DGMVN, 1995, *Geology of Vietnam*, department of geology and minerals of Vietnam, Hanoi: Science Publisher, v. v, p. 359.

- Faure, M., Lepvrier, C., Nguyen, V.V., Vu, T.V., Lin, W., and Chen, Z., 2014, The South China block-Indochina collision: Where, when, and how?: *Journal of Asian Earth Sciences*, v. 79, p. 260–274. doi:10.1016/j.jseae.2013.09.022.
- Faure, M., Nguyen, V.V., Hoai, L.T.T., and Lepvrier, C., 2018, Early Paleozoic or early-middle Triassic collision between the South China and Indochina blocks: The controversy resolved? Structural insights from the Kon Tum massif (central Vietnam): *Journal of Asian Earth Sciences*, v. 166, p. 162–180. doi:10.1016/j.jseae.2018.07.015.
- Findlay, R.H., and Trinh, P.T., 1997, The structural setting of the Song Ma region, Vietnam and the Indochina-south China plate boundary problem: *Gondwana Research*, v. 1, p. 11–33. doi:10.1016/s1342-937x(05)70003-4.
- Fu, S., Hu, R., Bi, X., Chen, Y., Yang, J., and Huang, Y., 2015, Origin of Triassic granites in central Hunan province, South China: Constraints from zircon U–pb ages and Hf and O isotopes: *International Geology Review*, v. 57, p. 97–111. doi:10.1080/00206814.2014.996258.
- Gao, W., Wang, Z., and Li, C., 2017, Triassic magmatism in the eastern part of the South China block: Geochronological and petrogenetic constraints from Indosinian granites: *Geoscience Frontiers*, v. 8, p. 445–456. doi:10.1016/j.gsf.2016.03.003.
- Gardner, C.J., Graham, I.T., Belousova, E., Booth, G.W., and Greig, A., 2017, Evidence for Ordovician subduction-related magmatism in the Truong Son terrane, SE Laos: Implications for Gondwana evolution and porphyry Cu exploration potential in SE Asia: *Gondwana Research*, v. 44, p. 139–156. doi:10.1016/j.gr.2016.11.003.
- Griffin, W., Wang, X., Jackson, S., Pearson, N., O'Reilly, S.Y., Xu, X., and Zhou, X., 2002, Zircon chemistry and magma mixing, SE China: in-situ analysis of Hf isotopes, Tonglu and Pingtan igneous complexes: *Lithos*, v. 61, p. 237–269. doi:10.1016/S0024-4937(02)00082-8.
- Hau, B.V., Kim, Y., Thanh, N.X., Hai, T.T., and Yi, K., 2018, Neoproterozoic deposition and Triassic metamorphism of metasedimentary rocks in the Nam Co complex, Song Ma suture zone, NW Vietnam: *Geosciences Journal*, v. 22, p. 549–568. doi:10.1007/s12303-018-0026-z.
- Hieu, P.T., Anh, N.T.Q., Minh, P., and Thuy, N.T.B., 2020, Geochemistry, zircon U–Pb ages and HF isotopes of the Muong Luan granitoid pluton, Northwest Vietnam and its petrogenetic significance: *The Island Arc*, v. 29, p. e12330. doi:10.1111/iar.12330.
- Hieu, P.T., Chen, F.-K., Thuy, N.T.B., Cường, N.Q., and Li, S.-Q., 2013, Geochemistry and zircon U–Pb ages and Hf isotopic composition of Permian alkali granitoids of the Phan Si Pan zone in northwestern Vietnam: *Journal of Geodynamics*, v. 69, p. 106–121. doi:10.1016/j.jog.2012.03.002.
- Hieu, P.T., Dung, N.T., Thuy, N.T.B., Minh, N.T., and Minh, P., 2016, U–pb ages and Hf isotopic composition of zircon and bulk rock geochemistry of the Dai Loc granitoid complex in Kontum massif: Implications for early Paleozoic crustal evolution in central Vietnam: *Journal of Mineralogical and Petrological Sciences*, v. 111, p. 326–336. doi:10.2465/jmps.151229.
- Hieu, P.T., Li, S.Q., Yu, Y., Thanh, N.X., Dung, L.T., Tu, V.L., Siebel, W., and Chen, F., 2017, Stages of late Paleozoic to early Mesozoic magmatism in the Song Ma belt, NW Vietnam: Evidence from zircon U–pb geochronology and Hf isotope composition: *International Journal of Earth Sciences*, v. 106, p. 855–874. doi:10.1007/s00531-016-1337-9.
- Hieu, P.T., Yang, Y.Z., Binh, D.Q., Nguyen, T.B.T., Dung, L.T., and Chen, F., 2015, Late Permian to early Triassic crustal evolution of the Kontum massif, central Vietnam: Zircon U–pb ages and geochemical and Nd–Hf isotopic composition of the Hai Van granitoid complex: *International Geology Review*, v. 57, p. 1877–1888. doi:10.1080/00206814.2015.1031194.
- Hoa, T.T., Anh, T.T., Phuong, N.T., Dung, P.T., Anh, T.V., Izokh, A. E., Borisenko, A.S., Lan, C.Y., Chung, S.L., and Lo, C.H., 2008a, Permo-Triassic intermediate–felsic magmatism of the Truong Son belt, eastern margin of Indochina: *Comptes Rendus Geoscience*, v. 340, p. 112–126. doi:10.1016/j.crte.2007.12.002.
- Hoa, T.T., Izokh, A.E., Polyakov, G.V., Borisenko, A.S., Anh, T.T., Balykin, P.A., Phuong, N.T., Rudnev, S.N., Van, V.V., and Nien, B.A., 2008b, Permo-Triassic magmatism and metallogeny of Northern Vietnam in relation to the Emeishan plume: *Russian Geology and Geophysics*, v. 49, p. 480–491. doi:10.1016/j.rgg.2008.06.005.
- Hoang, N.K., Quynh, A.N.T., Minh, P., Trung, H.P., and Thanh, T. N., 2023, Geochemistry and zircon U–Pb geochronology of the Dak Krong plutonic rocks in the Kontum massif (central Vietnam) and their petrogenetic implications: *Vietnam Journal of Earth Sciences*. doi:10.15625/2615-9783/18411.
- Hoskin, P.W., and Schaltegger, U., 2003, The composition of zircon and igneous and metamorphic petrogenesis: *Reviews in Mineralogy and Geochemistry*, v. 53, p. 27–62. doi:10.2113/0530027.
- Hung, D.D., Tsutsumi, Y., Hieu, P.T., Minh, N.T., Minh, P., Dung, N.T., Hung, N.B., Komatsu, T., Hoang, N., and Kawaguchi, K., 2022, Van Canh Triassic granite in the Kontum Massif, central Vietnam: Geochemistry, geochronology, and tectonic implications: *Journal of Asian Earth Sciences*, v. 7, p. 100075. doi:10.1016/j.jaesx.2021.100075.
- Hutchison, C.S., 1989, *Geological evolution of south-east Asia*, Volume 13: Oxford: Clarendon Press, p. 368.
- Jiang, W., Yu, J.H., Griffin, W., Pham, T., Qian, J., and Nguyen, D., 2023, Tectonic evolution of Southeast Asia documented by two periods of high-grade metamorphism in the Kon Tum Massif, Central Vietnam: *Lithos*, v. 454, p. 107277. doi:10.1016/j.lithos.2023.107277.
- Jiang, W., Yu, J.H., Wang, X., Griffin, W., Pham, T., Nguyen, D., and Wang, F., 2020, Early Paleozoic magmatism in northern Kontum Massif, Central Vietnam: Insights into tectonic evolution of the eastern Indochina block: *Lithos*, v. 376, p. 105750. doi:10.1016/j.lithos.2020.105750.
- Jiao, S.J., Li, X.H., Huang, H.Q., and Deng, X.G., 2015, Metasedimentary melting in the formation of charnockite: Petrological and zircon U–Pb–Hf–O isotope evidence from the Darongshan S-type granitic complex in southern China: *Lithos*, v. 239, p. 217–233. doi:10.1016/j.lithos.2015.10.004.
- Le Bas, M., and Streckeisen, A.L., 1991, The IUGS systematics of igneous rocks: *Journal of the Geological Society*, v. 148, p. 825–833. doi:10.1144/gsjgs.148.5.0825.
- Le, T.X., Dirks, P.H., Sanislav, I.V., Huizenga, J.M., Cocker, H.A., and Manestar, G.N., 2021, Geochronological constraints on the geological history and gold mineralization in the Tick Hill region, Mt Isa Inlier: *Precambrian Research*, v. 366, p. 106422. doi:10.1016/j.precamres.2021.106422.
- Lepvrier, C., Maluski, H., Van Tich, V., Leyreloup, A., Truong Thi, P., and Van Vuong, N., 2004, The early Triassic Indosinian orogeny in Vietnam (Truong Son belt and

- Kontum Massif); implications for the geodynamic evolution of Indochina: *Tectonophysics*, v. 393, p. 87–118. doi:10.1016/j.tecto.2004.07.030.
- Lepvrier, C., Maluski, H., Van Vuong, N., Roques, D., Axente, V., and Rangin, C., 1997, Indosinian NW-trending shear zones within the Truong Son belt (Vietnam) 40Ar-39Ar Triassic ages and Cretaceous to Cenozoic overprints: *Tectonophysics*, v. 283, p. 105–127. doi:10.1016/S0040-1951(97)00151-0.
- Lepvrier, C., Van Vuong, N., Maluski, H., Truong Thi, P., and Van Vu, T., 2008, Indosinian tectonics in Vietnam: *Comptes Rendus Geoscience*, v. 340, p. 94–111. doi:10.1016/j.crte.2007.10.005.
- Liu, J., Tran, M.D., Tang, Y., Nguyen, Q.L., Tran, T.H., Wu, W., Chen, J., Zhang, Z., and Zhao, Z., 2012, Permo-Triassic granitoids in the northern part of the Truong Son belt, NW Vietnam: Geochronology, geochemistry and tectonic implications: *Gondwana Research*, v. 22, p. 628–644. doi:10.1016/j.gr.2011.10.011.
- Liu, X., Wang, Q., Ma, L., Yang, J.H., Gou, G.N., Ou, Q., and Wang, J., 2020, Early Paleozoic intracontinental granites in the Guangzhou region of South China: Partial melting of a metasediment-dominated crustal source: *Lithos*, v. 376, p. 105763. doi:10.1016/j.lithos.2020.105763.
- Li, Y.J., Wei, J.H., Santosh, M., Tan, J., Fu, L.B., and Zhao, S.Q., 2016, Geochronology and petrogenesis of middle Permian S-type granitoid in southeastern Guangxi Province, South China: Implications for closure of the eastern paleo-Tethys: *Tectonophysics*, v. 682, p. 1–16. doi:10.1016/j.tecto.2016.05.048.
- Ludwig, K., 2003, User's manual for isoplot 3.00, a geochronological toolkit for Microsoft Excel: Berkeley geochronology center: Special Publication, v. 4, p. 25–32.
- Maluski, H., Lepvrier, C., Leyreloup, A., Tich, V.V., and Thi, P.T., 2005, 40Ar-39Ar geochronology of the charnockites and granulites of the Kan Nack complex, Kon Tum Massif, Vietnam: *Journal of Asian Earth Sciences* (English), v. 25, p. 653–677. doi:10.1016/j.jseae.2004.07.004.
- Maniar, P.D., and Piccoli, P.M., 1989, Tectonic discrimination of granitoids: *Geological Society of America Bulletin*, v. 101, p. 635–643. doi:10.1130/0016-7606(1989)101<0635:TDOG>2.3.CO;2.
- Metcalfe, I., 1998, Palaeozoic and Mesozoic geological evolution of the SE Asian region: multidisciplinary constraints and implications for biogeography, in Hall, R., and Holloway, J. D., eds., *Biogeography Geological Evolution of SE Asia: The Netherlands: Backhuys Publishers*, p. 25–41.
- Metcalfe, I., 2006, Palaeozoic and Mesozoic tectonic evolution and palaeogeography of East Asian crustal fragments: The Korean peninsula in context: *Gondwana Research*, v. 9, p. 24–46. doi:10.1016/j.gr.2005.04.002.
- Metcalfe, I., 2013, Gondwana dispersion and Asian accretion: Tectonic and palaeogeographic evolution of eastern Tethys: *Journal of Asian Earth Sciences*, v. 66, p. 1–33. doi:10.1016/j.jseae.2012.12.020.
- Minh, N.T., Dung, N.T., Hung, D.D., Minh, P., Yu, Y., and Hieu, P. T., 2020, Zircon U-Pb ages, geochemistry and isotopic characteristics of the Chu Lai granitic pluton in the Kontum Massif, central Vietnam: *Mineralogy and Petrology*, v. 114, p. 289–303. doi:10.1007/s00710-020-00707-x.
- Minh, P., Hieu, P.T., and Hoang, N.K., 2018, Geochemical and geochronological studies of the Muong Hum alkaline granitic pluton from the Phan Si Pan zone, northwest Vietnam: Implications for petrogenesis and tectonic setting: *The Island Arc*, v. 27, p. e12250. doi:10.1111/iar.12250.
- Minh, P., Hieu, P.T., Thuy, N.T.B., Dung, L.T., Kawaguchi, K., and Dung, P.T., 2021, Neoproterozoic granitoids from the Phan Si Pan zone, NW Vietnam: Geochemistry and geochronology constraints on reconstructing South China – India palaeogeography: *International Geology Review*, v. 63, p. 585–600. doi:10.1080/00206814.2020.1728584.
- Minh, P., Trung, H.P., Kawaguchi, K., Quynh, A.N.T., and Le Duc, P., 2022, Geochemistry, zircon U-Pb geochronology and Sr-nd-hf isotopic composition of the Cha Val plutonic rocks in central Vietnam: Implications for Permian-Triassic paleo-Tethys subduction-related magmatism: *Vietnam Journal of Earth Sciences*, v. 44, p. 301–326. doi:10.15625/2615-9783/16842.
- Nagy, E.A., Maluski, H., Lepvrier, C., Schärer, U., Thi, P.T., Leyreloup, A., and Tich, V.V., 2001, Geodynamic significance of the Kontum Massif in central Vietnam: Composite 40Ar/39Ar and U-Pb ages from Paleozoic to Triassic: *The Journal of Geology*, v. 109, p. 755–770. doi:10.1086/323193.
- Nakano, N., Osanai, Y., Minh, N.T., Miyamoto, T., Hayasaka, Y., and Owada, M., 2008, Discovery of high-pressure granulite-facies metamorphism in northern Vietnam: Constraints on the permo-Triassic Indochinese continental collision tectonics: *Comptes Rendus Geoscience*, v. 340, p. 127–138. doi:10.1016/j.crte.2007.10.013.
- Nakano, N., Osanai, Y., Owada, M., Binh, P., Hokada, T., Kaiden, H., and Bui, V.T., 2021, Evolution of the Indochina block from its formation to amalgamation with Asia: Constraints from protoliths in the Kontum Massif, Vietnam: *Gondwana Research*, v. 90, p. 47–62. doi:10.1016/j.gr.2020.11.002.
- Nakano, N., Osanai, Y., Sajeev, K., Hayasaka, Y., Miyamoto, T., Minh, N.T., Owada, M., and Windley, B., 2010, Triassic eclogite from northern Vietnam: inferences and geological significance: *Journal of Metamorphic Geology*, v. 28, p. 59–76. doi:10.1111/j.1525-1314.2009.00853.x.
- Nam, T.N., Toriumi, M., Sano, Y., Terada, K., and Thang, T.T., 2003, 2.9, 2.36, and 1.96 Ga zircons in orthogneiss south of the red river shear zone in Viet Nam: Evidence from SHRIMP U-pb dating and tectonothermal implications: *Journal of Asian Earth Sciences*, v. 21, p. 743–753. doi:10.1016/S1367-9120(02)00089-5.
- Ngo, X.T., Bui, H.V., Tran, D.M., Kim, Y., Xiaochun, L., Tran, H.T., and Khang, L.Q., 2023, Ordovician continental arc magmatism in the Tam Ky-Phuoc Son Suture Zone, Central Indochina Block, Southeast Asia: *Geological Journal*, v. 58, no. 2, p. 825–836. doi:10.1002/gj.4626
- Osanai, Y., Nakano, N., Owada, M., Nam, T.N., Miyamoto, T., Minh, N.T., Nam, N.V., and Tri, T.V., 2008, Collision zone metamorphism in Vietnam and adjacent South-eastern Asia: Proposition for trans Vietnam orogenic belt: *Journal of Mineralogical and Petrological Sciences*, v. 103, p. 226–241. doi:10.2465/jmps.080620e.
- Pearce, J., 1983, The role of sub-continental lithosphere in magma genesis at destructive plate margins, in Hawkesworth, C.J., and Norry, M.J., eds., *Continental Basalts and Mantle Xenoliths: Nantwich: Shiva*, p. 230–249.
- Pearce, J.A., Harris, N.B., and Tindle, A.G., 1984, Trace element discrimination diagrams for the tectonic interpretation of granitic rocks: *Journal of Petrology*, v. 25, p. 956–983. doi:10.1093/petrology/25.4.956.



- Peccerillo, A., and Taylor, S., 1976, Geochemistry of Eocene calc-alkaline volcanic rocks from the Kastamonu area, Northern Turkey: Contributions to Mineralogy and Petrology, v. 58, p. 63–81. doi:10.1007/BF00384745.
- Pettke, T., 2008, Analytical protocols for element concentration and isotope ratio measurements in fluid inclusions by LA-(MC)-ICP-MS: Laser ablation ICP-MS in the earth sciences: Current practices outstanding issues: Mineralogical Association of Canada, Short Course Series, v. 40, p. 189–218.
- Qian, X., Wang, Y., Zhang, Y., Zhang, Y., Senebottalath, V., Zhang, A., and He, H., 2019, Petrogenesis of Permian–Triassic felsic igneous rocks along the truong son zone in northern Laos and their paleotethyan assembly: Lithos, v. 328–329, p. 101–114. doi:10.1016/j.lithos.2019.01.006.
- Roger, F., Jolivet, M., Maluski, H., Respaut, J.P., Münch, P., Paquette, J.L., Vu Van, T., and Nguyen Van, V., 2014, Emplacement and cooling of the dien bien phu granitic complex: Implications for the tectonic evolution of the dien bien phu fault (truong son belt, NW Vietnam): Gondwana Research, v. 26, p. 785–801. doi:10.1016/j.gr.2013.07.018.
- Roger, F., Maluski, H., Leyreloup, A., Lepvrier, C., and Truong Thi, P., 2007, U–pb dating of high temperature metamorphic episodes in the Kon Tum massif (Vietnam): Journal of Asian Earth Sciences, v. 30, p. 565–572. doi:10.1016/j.jseae.2007.01.005.
- Sang, Đ.Q., 2011, PETrographic characteristics and zircon u–pb geochronology of granitoid rocks in the southern bên giang, qung nam province: Science & Technology Development, v. 14, p. 17–30. in Vietnamese with English abstract. doi:10.32508/stdj.v14i4.2024.
- Scherer, E., Munker, C., and Mezger, K., 2001, Calibration of the lutetium–hafnium clock: Science, v. 293, p. 683–687. doi:10.1126/science.1061372.
- Shi, M.F., Lin, F.C., Fan, W.Y., Deng, Q., Cong, F., Tran, M.D., Zhu, H.P., and Wang, H., 2015, Zircon U–pb ages and geochemistry of granitoids in the truong son terrane, Vietnam: Tectonic and metallogenic implications: Journal of Asian Earth Sciences, v. 101, p. 101–120. doi:10.1016/j.jseae.2015.02.001.
- Song, Z.T., and Xu, X.S., 2022, Petrogenesis of high-maficity S-type granites: Insight from the early Paleozoic Jinxi granite, South China: Lithos, v. 412, p. 106597. doi:10.1016/j.lithos.2022.106597.
- Sun, S.S., and McDonough, W.F., 1989, Chemical and isotopic systematics of oceanic basalts: Implications for mantle composition and processes: Geological Society, London, Special Publications, v. 42, p. 313–345. doi:10.1144/GSL.SP.1989.042.01.19.
- Thanh, T.V., Hieu, P.T., Minh, P., Nhuan, D.V., and Thuy, N.T.B., 2019, Late Permian–Triassic granitic rocks of Vietnam: The muong lat example: International Geology Review, v. 61, p. 1823–1841. doi:10.1080/00206814.2018.1561335.
- Thanh, N.X., Tu, M.T., Itaya, T., and Kwon, S., 2011, Chromian-spinel compositions from the Bo Xinh ultramafics, Northern Vietnam: Implications on tectonic evolution of the Indochina block: Journal of Asian Earth Sciences, v. 42, p. 258–267. doi:10.1016/j.jseae.2011.02.004.
- Thục, Đ.Đ., and Trung, H., 1995, Geology of Vietnam-volume II: Magma formations: Vietnam Geology Department, v. v, p. 359.
- Trang, N.V., 1994, Geological and mineral map of Vietnam at scale 1:200 000 of the Ba Na sheet Geological survey and mineral of Viet Nam: Hanoi.
- Tran, H.T., Zaw, K., Halpin, J.A., Manaka, T., Meffre, S., Lai, C.K., Lee, Y., Le, H.V., and Dinh, S., 2014, The tam Ky-Phuoc son shear zone in central Vietnam: Tectonic and metallogenic implications: Gondwana Research, v. 26, p. 144–164. doi:10.1016/j.gr.2013.04.008.
- Tri, T.V., and Khuc, V., 2011, Geology and earth resources of Vietnam: Ha Noi, Vietnam, Publishing House for Science and Technology, p. 634.
- Trong, N.H., Zong, K., Liu, Y., Yuan, Y., Hieu, P.T., Dung, L.T., and Minh, P., 2021, Early Paleozoic arc magmatism and accretionary orogenesis in the Indochina block, Southeast Asia: The Journal of Geology, v. 129, p. 33–48. doi:10.1086/713727.
- Usuki, T., Lan, C.Y., Tran, T.H., Pham, T.D., Wang, K.L., Shellnutt, G.J., and Chung, S.L., 2015, Zircon U–pb ages and Hf isotopic compositions of alkaline silicic magmatic rocks in the phan Si pan-tu Le region, northern Vietnam: Identification of a displaced western extension of the emeishan large igneous province: Journal of Asian Earth Sciences, v. 97, p. 102–124. doi:10.1016/j.jseae.2014.10.016.
- Usuki, T., Lan, C.Y., Yui, T.F., Iizuka, Y., Van Vu, T., Tran, T.A., Okamoto, K., Wooden, J.L., and Liou, J.G., 2009, Early Paleozoic medium-pressure metamorphism in central Vietnam: evidence from SHRIMP U–Pb zircon ages: Geosciences Journal, v. 13, p. 245–256. doi:10.1007/s12303-009-0024-2.
- Wang, S., Mo, Y., Wang, C., and Ye, P., 2016, Paleotethyan evolution of the Indochina block as deduced from granites in northern Laos: Gondwana Research, v. 38, p. 183–196. doi:10.1016/j.gr.2015.11.011.
- Wang, Y., Wang, Y., Qian, X., Zhang, Y., Gan, C., Senebottalath, V., and Wang, Y., 2020, Early Paleozoic subduction in the Indochina interior: Revealed by Ordo–Silurian mafic-intermediate igneous rocks in South Laos: Lithos, v. 362, p. 105488. doi:10.1016/j.lithos.2020.105488.
- Watson, E.B., and Harrison, T.M., 1983, Zircon saturation revisited: Temperature and composition effects in a variety of crustal magma types: Earth and Planetary Science Letters, v. 64, p. 295–304. doi:10.1016/0012-821X(83)90211-X.
- Whalen, J.B., Currie, K.L., and Chappell, B.W., 1987, A-type granites: geochemical characteristics, discrimination and petrogenesis: Contributions to Mineralogy and Petrology, v. 95, p. 407–419. doi:10.1007/BF00402202.
- Wu, F.Y., Yang, Y.H., Xie, L.W., Yang, J.H., and Xu, P., 2006, Hf isotopic compositions of the standard zircons and baddeleyites used in U–pb geochronology: Chemical Geology, v. 234, p. 105–126. doi:10.1016/j.chemgeo.2006.05.003.
- Xiao, Q.R., Wang, Q., Liu, Z.Y., Xiong, F.H., Fan, L., Zhao, H., and Gong, T.T., 2023, Petrogenesis and tectonic implications of the early Paleozoic granites in the lincang granitic batholith, southwestern China: Constraints from geochronology, geochemistry and Hf isotopes: Ore and Energy Resource Geology, v. 1, p. 100022. doi:10.1016/j.oreoa.2023.100022.
- Xu, W.C., Luo, B.J., Xu, Y.J., Wang, L., and Chen, Q., 2018, Geochronology, geochemistry, and petrogenesis of late Permian to early Triassic mafic rocks from Darongshan, South China: Implications for ultrahigh-temperature metamorphism and S-type granite generation: Lithos, v. 308, p. 168–180. doi:10.1016/j.lithos.2018.03.004.

- Yu, Y., Huang, X.L., He, P.L., and Li, J., 2016, I-type granitoids associated with the early Paleozoic intracontinental orogenic collapse along pre-existing block boundary in South China: *Lithos*, v. 248, p. 353–365. doi:[10.1016/j.lithos.2016.02.002](https://doi.org/10.1016/j.lithos.2016.02.002).
- Żelaźniewicz, A., Hòà, T.T., and Larionov, A.N., 2013, The significance of geological and zircon age data derived from the wall rocks of the Ailao Shan–red river shear zone, NW Vietnam: *Journal of Geodynamics*, v. 69, p. 122–139. doi:[10.1016/j.jog.2012.04.002](https://doi.org/10.1016/j.jog.2012.04.002).
- Zhang, R.Y., Lo, C.H., Chung, S.L., Grove, M., Omori, S., Iizuka, Y., Liou, J.G., and Tri, T.V., 2013, Origin and tectonic implication of ophiolite and eclogite in the song ma suture zone between the South China and Indochina blocks: *Journal of Metamorphic Geology*, v. 31, p. 49–62. doi:[10.1111/jmg.12012](https://doi.org/10.1111/jmg.12012).
- Zhong, Y., Ma, C., Zhang, C., Wang, S., She, Z., Liu, L., and Xu, H., 2013, Zircon U-Pb age, Hf isotopic compositions and geochemistry of the Silurian fengdingshan I-type granite pluton and Taoyuan mafic-felsic complex at the southeastern margin of the Yangtze block: *Journal of Asian Earth Sciences*, v. 74, p. 11–24. doi:[10.1016/j.jseas.2013.05.025](https://doi.org/10.1016/j.jseas.2013.05.025).
- Zhou, X., Yu, J.-H., O'Reilly, S.Y., Griffin, W.L., Wang, X., and Sun, T., 2017, Sources of the nanwenhe-song chay granitic complex (SW China-NE Vietnam) and its tectonic significance: *Lithos*, v. 290–291, p. 76–93. doi:[10.1016/j.lithos.2017.07.017](https://doi.org/10.1016/j.lithos.2017.07.017).